

EXPERIMENTAL STUDY OF RADIOLYTIC OXYGEN REMOVAL  
IN IRRADIATED SAMPLES



A Thesis Submitted in Partial Fulfillment of the Requirements for the  
Degree of Master of Science in Physics  
Suranaree University of Technology  
Academic Year 2022

การศึกษาทดลองการกำจัดออกซิเจนด้วยรังสีในตัวอย่างที่ถูกฉายด้วยรังสี



วิทยานิพนธ์นี้เป็นส่วนหนึ่งของการศึกษาตามหลักสูตรปริญญาวิทยาศาสตรมหาบัณฑิต  
สาขาวิชาฟิสิกส์  
มหาวิทยาลัยเทคโนโลยีสุรนารี  
ปีการศึกษา 2565

EXPERIMENTAL STUDY OF RADIOLYTIC OXYGEN REMOVAL  
IN IRRADIATED SAMPLES

Suranaree University of Technology has approved this thesis submitted in partial fulfillment of the requirements for a Master's Degree.

Thesis Examining Committee



(Assoc. Prof. Dr. Panomsak Meemon)

Chairperson



(Asst. Prof. Dr. Chinorat Kobdaj)

Member (Thesis Advisor)



(Assoc. Prof. Dr. Chutima Talabnin)

Member (Thesis Co-advisor)



(Asst. Prof. Dr. Christoph Herold)

Member



(Dr. Martina Christina Fuss)

Member



(Assoc. Prof. Dr. Chatchai Jothityangkoon)

Vice Rector for Academic Affairs  
and Quality Assurance



(Prof. Dr. Santi Maensiri)

Dean of Institute of Science

แพรวา การุญ : การศึกษาทดลองการกำจัดออกซิเจนด้วยรังสีในตัวอย่างที่ถูกฉายด้วยรังสี  
(EXPERIMENTAL STUDY OF RADIOLYTIC OXYGEN REMOVAL IN IRRADIATED  
SAMPLES) อาจารย์ที่ปรึกษา : ผู้ช่วยศาสตราจารย์ ดร.ชินรัตน์ กอบเดช, 73 หน้า.

คำสำคัญ: การฉายรังสีแบบแฟลช/ ผลกระทบจากการฉายรังสีแบบแฟลช/ การกำจัดออกซิเจน

ในช่วงหลายปีที่ผ่านมาการรักษาโรคมะเร็งด้วยการรักษาด้วยรังสีแบบแฟลชได้รับความสนใจเป็นอย่างมาก เนื่องจากมีผลการทดลองที่แสดงถึงการปกป้องเนื้อเยื่อปกติจากการทำลายของรังสีที่เกิดขึ้นจากการฉายรังสีแบบแฟลช แต่กลไกภายใต้ผลกระทบจากการฉายรังสีแบบแฟลชยังไม่ได้รับการยืนยันที่แน่ชัด หนึ่งในสมมติฐานที่ถูกนำมาพิสูจน์และเชื่อว่าสามารถใช้อธิบายผลกระทบจากการฉายรังสีแบบแฟลชได้คือ สมมติฐานการกำจัดออกซิเจนและปฏิกิริยาเคมีที่เกิดขึ้นในการฉายรังสีวิทยานิพนธ์นี้จึงมีจุดประสงค์เพื่อตรวจสอบสมมติฐานการกำจัดออกซิเจนโดยทำการทดลองการฉายรังสีด้วยสองช่วงอัตราปริมาณรังสีที่แตกต่างกันและฉายรังสีในตัวอย่างที่แตกต่างกัน ในส่วนแรกตัวอย่างที่เตรียมไว้ถูกฉายด้วยรังสีเอกซ์ด้วยปริมาณรังสี 50 เกรย์ต่อการฉายหนึ่งครั้ง ที่อัตราปริมาณรังสีแบบดั้งเดิม 4.5 – 10.4 เกรย์ต่อนาที โดยใช้หัวตรวจวัดรังสีชนิด Semiflex ionization chamber เพื่อตรวจวัดรังสี ผลการทดลองแสดงให้เห็นว่าออกซิเจนถูกกำจัดออกอย่างต่อเนื่องและมีค่าเฉลี่ยสูงที่สุดในการฉายขั้นแรกและลดลงในการฉายขั้นถัดไป คาดว่าอนุมูลเคมีที่ยังคงเหลืออยู่หลังจากการฉายรังสีในขั้นแรกสามารถทำปฏิกิริยากับอนุมูลเคมีที่ถูกสร้างขึ้นใหม่ในการฉายรังสีในขั้นถัดมา เป็นผลให้เกิดการทำปฏิกิริยาระหว่างอนุมูลเคมีนั้นและลดปฏิกิริยาที่มีออกซิเจนเป็นส่วนร่วม จึงเป็นสาเหตุที่ทำให้ออกซิเจนถูกกำจัดได้ลดลง ส่วนการฉายรังสีแบบแฟลช ตัวอย่างถูกฉายด้วยลำอิเล็กตรอนที่ถูกเร่งด้วยเลเซอร์ซึ่งอัตราปริมาณรังสีต่อหนึ่งรอบฉายคือประมาณ 30 เกรย์ ต่อ 20 พิโควินาที โดยใช้ XD radiochromic films (RCFs) สำหรับการตรวจวัดรังสี ผลการทดลองพบว่าระดับของออกซิเจนลดลงอย่างรวดเร็วหลังจากการฉายรังสี ซึ่งปัจจุบันยังคงทราบเพียงปริมาณออกซิเจนที่ถูกกำจัดออกไปในแต่ละครั้งของการฉายรังสี ข้อมูลปริมาณรังสีจากการทดลองการฉายรังสีแบบแฟลชยังคงอยู่ในขั้นตอนการวิเคราะห์ผลโดยใช้การจำลอง Monte Carlo เพื่อให้สามารถเปรียบเทียบผลการกำจัดออกซิเจนจากการฉายรังสีทั้งสองช่วงอัตราปริมาณรังสีที่แตกต่างกันได้ในลำดับถัดไป

สาขาวิชาฟิสิกส์  
ปีการศึกษา 2565

ลายมือชื่อนักศึกษา แพรวา การุญ  
ลายมือชื่ออาจารย์ที่ปรึกษา ชินรัตน์ กอบเดช

PHAREWA KAROON : EXPERIMENTAL STUDY OF RADIOLYTIC OXYGEN REMOVAL IN IRRADIATED SAMPLES. THESIS ADVISOR : ASST. PROF. CHINORAT KOBDAJ, Ph.D. 73 PP.

Keyword: FLASH irradiation/ FLASH effect/ oxygen depletion

Cancer treatment with FLASH radiotherapy has sparked a lot of interest over the years due to experimental studies that have shown a sparing effect on normal tissues from FLASH irradiation. However, the mechanism behind the FLASH effect has not been conclusively confirmed. One of the hypotheses that has been proven and believed to explain FLASH effect is the oxygen depletion hypothesis and the chemical reactions occurring in irradiation. The purpose of this thesis is to verify the oxygen removal during the irradiation by conducting radiation experiments with two different dose rate ranges on different samples. The prepared samples were irradiated using X-ray beam with a total of 50 Gray (Gy) per irradiation at the conventional dose rates of 4.5–10.4 Gy/min. A Semiflex chamber has been used for the dosimetry in this setup. The experimental results demonstrated that oxygen was continuously eliminated during the irradiation. The values of average oxygen removal are highest in the first irradiation step and then decrease in the steps afterward. The prediction is the remaining chemical radicals after the initial irradiation can react with the new chemical radicals generated in the next irradiation, resulting in the interaction between those chemical radicals and reducing the interaction with oxygen thereby decreasing the amount of removed oxygen. Next for the FLASH irradiation, the samples were irradiated with a laser-accelerated electron at a dose of approximately 30 Gy in 20 picoseconds (ps) using XD radiochromic films (RCFs) as the dosimetry. The experimental results showed that oxygen levels dropped sharply after irradiation. Only the amount of oxygen is removed with each irradiation is known. The dose data from the FLASH irradiation experiment is still being analyzed using Monte Carlo simulations, so the

effects of two different dose rate ranges on oxygen depletion will be explored in further study.



School of Physics  
Academic Year 2022

Student's Signature บวรวิทย์ มฤตยู  
Advisor's Signature C. Kobdaj

## ACKNOWLEDGEMENTS

Firstly, I would like to express my sincere thanks to my respected advisor, Asst. Prof. Dr. Chinorat Kobdaj, who took the opportunity and pushed me to do this project. He has helped me to make decisions and overcome my fears. I was able to complete my thesis partly thanks to his support.

Additionally, I would like to thank my kind co-advisor, Assoc. Prof. Dr. Chutima Talabnin for her advice on everything about the biology and chemistry parts.

I would like to thank my supervisor Dr. Martina Fuß for her teaching and guidance since the beginning of the project. When I have doubts or questions, she always gives me sound advice and explains things to me calmly.

I am very grateful to the GET INvolved program for the great opportunities. I would like to thank everyone at GSI, consisting of every researcher, every colleague and every person in the International Office. I have a very great experience with the great collaboration. Everyone there assisted me in every way.

I would like to thank the Development Promotion of Science and Technology (DPST) Scholarship for partial support. It gives ordinary students like me to gain a lot of special opportunities.

I would like to thank Miss Dea Aulia Kartini for her help in explaining many things that make me confused, for her comments, and for helping to improve my thesis.

Finally, I am so grateful to my family, friends, and the person who is always by my side for encouragement and support.

Pharewa Karoon

# CONTENTS

	Page
ABSTRACT IN THAI . . . . .	I
ABSTRACT IN ENGLISH . . . . .	II
ACKNOWLEDGEMENTS . . . . .	IV
CONTENTS . . . . .	V
LIST OF TABLES . . . . .	VII
LIST OF FIGURES . . . . .	VIII
LIST OF ABBREVIATIONS . . . . .	XI
<b>CHAPTER</b>	
<b>I INTRODUCTION . . . . .</b>	<b>1</b>
<b>II BACKGROUND AND KNOWLEDGE . . . . .</b>	<b>4</b>
2.1 Radiotherapy . . . . .	4
2.1.1 Electron and X-ray radiation . . . . .	4
Electron radiation . . . . .	5
X-ray radiation . . . . .	5
2.1.2 The absorbed dose . . . . .	6
2.1.3 Water radiolysis . . . . .	7
2.2 Tumor Oxygenation . . . . .	8
2.2.1 Oxygen transport to tissue . . . . .	8
2.2.2 Hypoxic tumors . . . . .	9
2.3 FLASH irradiation . . . . .	10
2.3.1 FLASH effect . . . . .	12
2.3.2 Oxygenation and oxygen depletion . . . . .	13
<b>III MATERIAL AND METHODS . . . . .</b>	<b>18</b>
3.1 Instruments for oxygen measurement . . . . .	18
3.1.1 The measurement principle . . . . .	19
3.1.2 Container setups . . . . .	20
3.1.3 Samples preparation . . . . .	22
3.2 Sensor calibration . . . . .	22
3.3 Irradiation modalities . . . . .	24

## CONTENTS (Continued)

	Page
3.3.1 PHELIX laser . . . . .	25
3.4 Experimental Setup and Dosimetry . . . . .	26
3.4.1 X-ray irradiation setup . . . . .	26
3.4.2 Laser-accelerated electron irradiation setup . . . . .	27
3.4.3 Dosimetry . . . . .	27
ionization chamber . . . . .	27
Radiochromic films . . . . .	29
Thermoluminescent dosimeters . . . . .	29
<b>IV PRELIMINARY TEST . . . . .</b>	<b>30</b>
4.1 Dosimetry Test . . . . .	30
4.2 Preliminary results . . . . .	32
<b>V RESULTS . . . . .</b>	<b>35</b>
5.1 Oxygen removal in X-ray irradiation . . . . .	35
5.2 The irradiated samples from the PHELIX laser-accelerated electrons . . . . .	46
<b>VI CONCLUSION AND DISCUSSION . . . . .</b>	<b>52</b>
REFERENCES . . . . .	54
APPENDICES	
APPENDIX A CALIBRATION FOR EXPERIMENT . . . . .	61
A.1 Calibration for X-ray irradiation experiment . . . . .	61
A.2 Calibration for laser-accelerated electrons ir- radiation experiment . . . . .	62
APPENDIX B CONFERENCES AND PRESENTATIONS . . . . .	63
B.1 List of oral presentation . . . . .	63
CURRICULUM VITAE . . . . .	73

## LIST OF TABLES

Table		Page
4.1	List of correction factors according to the position of container and dosimeter during irradiation . . . . .	32
4.2	The average oxygen removal from the preliminary experiment with the X-ray irradiation . . . . .	34
5.1	The average oxygen removal per dose of full oxygenated water	42
5.2	The average oxygen removal per dose of Deoxygenated water	43
5.3	The average oxygen removal per dose of irradiated PBS samples in large container . . . . .	43
5.4	The average oxygen removal per dose of irradiated culture medium samples . . . . .	43
5.5	The average oxygen removal per dose of irradiated lysed cell samples . . . . .	44
5.6	The average oxygen removal per dose of irradiated full oxygenated water samples with discrete irradiation. . . . .	44
5.7	The average oxygen removal of irradiated samples in four different types of samples from PHELIX laser-accelerated electron experiments . . . . .	49
5.8	The average oxygen removal of irradiated samples from PHELIX laser-accelerated electron after estimating the radiation dose . . . . .	51
A.1	Cal 0 and Cal 100 calibration of P1 and P5 containers . . . . .	61
A.2	Cal 0 and Cal 100 calibration for a small container . . . . .	61
A.3	Cal 0 and Cal 100 calibration of a small container in the vacuum condition . . . . .	62

## LIST OF FIGURES

Figure		Page
1.1	The comparison between normal tissue and tumor tissue that responds to the different irradiations, conventional and FLASH radiotherapy . . . . .	2
2.1	The main reactions take place during water radiolysis. . . . .	8
2.2	Oxygen is transported to tissue cells by using the hemoglobin protein in the red blood cell. . . . .	9
2.3	A bunch of cancer cells spreads out to nearby normal cells . . . . .	10
2.4	Tumor microenvironment . . . . .	11
2.5	A microscopic visualization of mini pig skin irradiation . . . . .	14
2.6	A microscopic evolution of the lesion in the cat patient . . . . .	15
2.7	The progress of tumor lesion on the human arm before and after treatment . . . . .	16
2.8	Surviving fraction of <i>E.coli B/r</i> bacteria using a shot-pulsed irradiation . . . . .	17
2.9	The survival fraction of prostate cancer cells at different doses under normoxic and hypoxic conditions . . . . .	17
3.1	Oxygen meter . . . . .	19
3.2	Jablonski diagram . . . . .	20
3.3	A container was filled with the sample for X-ray irradiation. . . . .	23
3.4	Samples for electron irradiation using the PHELIX laser and some experiments with X-ray irradiation . . . . .	24
3.5	The experiment area of PHELIX laser building . . . . .	25
3.6	Experimental setup for X-ray irradiation . . . . .	26
3.7	Experimental setup for laser-accelerated electron irradiation . . . . .	28
4.1	A preliminary result from X-ray irradiation . . . . .	33

## LIST OF FIGURES (Continued)

Figure		Page
5.1	An example graph of the oxygen concentration during three steps of X-ray irradiation in full oxygenated water . . . . .	36
5.2	An example graph of the oxygen concentration during three steps of X-ray irradiation in deoxygenated water . . . . .	37
5.3	An example graph of the oxygen concentration during three steps of X-ray irradiation in PBS . . . . .	37
5.4	An example graph of the oxygen concentration during three steps of X-ray irradiation in cell culture medium . . . . .	38
5.5	An example graph of the oxygen concentration during two steps of X-ray irradiation in lysed cells . . . . .	38
5.6	The oxygen removal per dose in each irradiation step of full oxygenated water and deoxygenated water . . . . .	39
5.7	The oxygen removal per dose of irradiated PBS samples compared to the given dose. . . . .	40
5.8	The oxygen removal per dose of irradiated cell culture medium samples compared to the given dose. . . . .	40
5.9	The oxygen removal per dose of irradiated samples compared to the given dose. . . . .	41
5.10	Comparison of the cumulative doses and the average oxygen removal in all sample types. . . . .	42
5.11	The oxygen removal per dose in irradiated water samples in comparison with the irradiated time of discrete irradiation. . . . .	45
5.12	The graph examples of the oxygen removal in irradiated water and PBS from the irradiation by PHELIX laser-accelerated electrons. . . . .	47
5.13	The graph examples of the oxygen removal in irradiated cell culture medium and lysed cells from the irradiation by PHELIX laser-accelerated electrons. . . . .	48
5.14	The oxygen removal in irradiated samples after irradiation with laser-accelerated electrons in each shot. . . . .	49

## LIST OF FIGURES (Continued)

Figure		Page
5.15	The average oxygen removal in irradiated samples after irradiation with laser-accelerated electrons . . . . .	50
5.16	The average oxygen removal of irradiated samples from PHELIX laser-accelerated electron after estimating the radiation dose . . . . .	50
B.1	The certificate of participation in the Siam Physics Congress 2022 . . . . .	63
B.2	The certificate of participation in the RSU conference 2023 . . . . .	64



## LIST OF ABBREVIATIONS

CONV-RT	Conventional Radiotherapy
DLA	Direct Laser Acceleration
FAIR	Facility for Antiproton and Ion Research
FLASH-RT	FLASH Radiotherapy
GSI	Gesellschaft für schwerionenforschung
LED	Light Emitting Diode
NCD	Near Critical Density
PBS	Phosphate Buffer Saline
PEEK	Polyetheretherketone
PHELIX	The Petawatt High-Energy Laser for Heavy Ion EXperiments
PMMA	PolyMethylMethAcrylate
POF	Polymer Optical Fiber
RCF	Radiochromic Film
RT	Radiotherapy or Radiation Therapy
TAC	Triacetate Cellulose
TLD	Thermoluminescent Dosimeter
Gy	Gray
ns	Nanosecond
ps	Picosecond
s	Second
min	Minute
$\mu$ M	Micromolar
hr	Hour
mm	Millimeter
kV	Kilovolt
eV	Electron volt
MeV	Megaelectron volt
J	Joule
kJ	Kilojoule

# CHAPTER I

## INTRODUCTION

Radiotherapy or radiation therapy (RT) is currently one of the main techniques used to cure cancer. RT utilizes ionizing radiation to kill cancer cells where ions transfer their energy to the cells and change the genetic structure of deoxyribonucleic acid (DNA), making the DNA unable to repair itself and resulting in cancer cell death. The typical RT, we have been using currently, is also known as conventional irradiation or conventional radiotherapy (CONV-RT). In conventional radiotherapy, the irradiation treatment is performed using a dose rate in the low dose rate range, with a value around 0.03 Gy/s. Although the CONV-RT is widely accepted for cancer treatment at present, RT is still being developed to increase treatment channels for patients. In the last decade, ultra-high dose rate irradiation has gained more attention on the strong antitumor effect and the sparing effect on healthy tissues. This irradiation was coined in 2014 and is called FLASH irradiation (Favaudon et al., 2014) for the dose rates in the range of 40 Gy/s or higher. An early study in mammalian cells discovered that when the total dose was delivered within a single nanosecond frame time, cell survival increased when compared to the conventional treatment (Epp et al., 1972). One of the obvious results is a study with an *in vivo* experiment on normal mini-pig skin and the cat patients that have cancer cells on their nasal planum (Vozenin et al., 2019). The results have been confirmed that the treatment with the FLASH dose rate is effective in protecting the normal tissues. The FLASH treatment in the first human patient also went well (Bourhis et al., 2019). Therefore, FLASH treatment is one of the exciting and expected methods to increase the therapeutic window. The response of the irradiated tissues using CONV-RT and FLASH irradiation were compared in the figure 1.1. However, the mechanism underlying the FLASH effect remains unconfirmed. One of the expected hypotheses to explain the FLASH effect is the oxygen removal during FLASH irradiation.

Oxygen is one of the most necessary gases for all living things, including humans. Our cells have to use oxygen for the cellular respiration process to

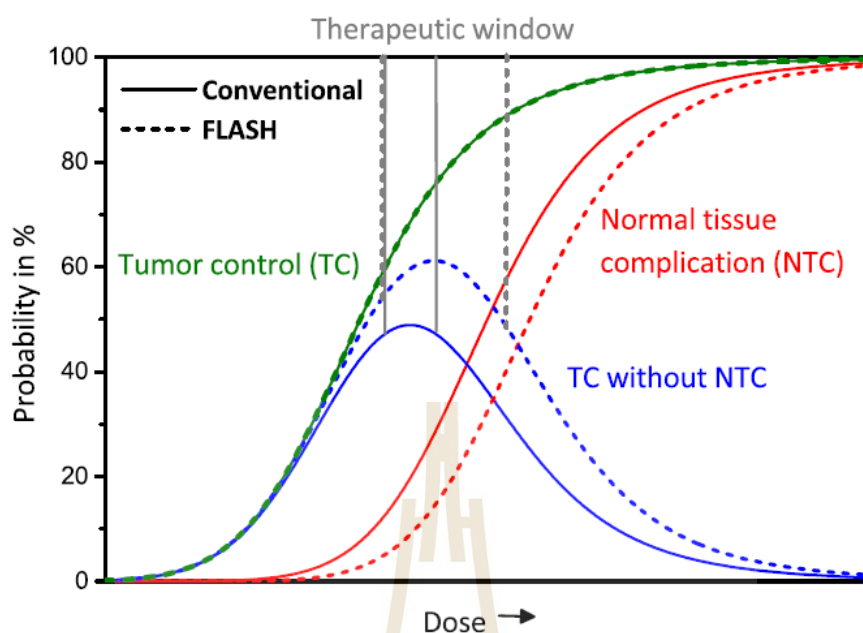


**Figure 1.1** The comparison between normal tissue and tumor tissue that responds to the different irradiations, conventional (CONV, solid lines) and FLASH (dashed lines) radiotherapy. The tumor control probability (TCP, green) is similar at the same dose for both CONV and FLASH radiotherapy. In contrast to the normal tissue, the complication probability (NTCP, red) on the FLASH radiotherapy is lower than on the CONV radiotherapy. The maximum range of TCP without NTCP is called the therapeutic window (Schüller et al., 2020).

produce the energy needed for our activities. Dissolved oxygen in our bodies is also a biological parameter that qualifies as a good radiosensitizer during irradiation (Zakaria et al., 2020). The irradiation experiments show the hypoxic tumors have more radiation resistance than that of the well-oxygenated tumors, with an oxygen enhancement ratio (OER) of 2-3 (Pettersson K, 2020). When ionizing radiation passes through water, it creates a variety of ionic and excited states that further break down to produce radiolytic products such as  $e_{aq}^-$ ,  $H^\bullet$ ,  $OH^\bullet$ ,  $H_2O_2$ ,  $H_2$  and  $H_3O^+$  in short timescales (Le Caër, 2011). A short time later, some of the products, which are solvated electrons ( $e_{aq}^-$ ) and hydrogen radicals  $H^\bullet$ , react with the dissolved molecular oxygen and then form the superoxide  $O_2^{\bullet-}$  and perhydroxyl radicals  $HO_2^{\bullet-}$  resulting in a decrease in dissolved oxygen as shown

in equations 1.1 and 1.2 (Boscolo et al., 2021; Pastina and LaVerne, 2001).



Under the oxygen depletion hypothesis, the FLASH effect was expected to be caused by the prompt radiochemical reactions that occur in the irradiated tissues. In the short time frame of the irradiation, the dissolved oxygen in the tissues is rapidly removed. The oxygen surrounding the tissues cannot replace it in time and this makes the tissues going into a transient state of the hypoxic environment. As a result, radiation resistance in tissues has increased, resulting in normal tissues being spared from FLASH irradiation. Early bacterial studies have revealed that the oxygen removal can result in considerable sparing at very high dose rates (Dewey, 1959; Weiss et al., 1974). Many studies of *in vitro* experiments have been performed to consider the oxygen depletion hypothesis of the FLASH effect (Adrian et al., 2019). However, the current analysis using the computational model revealed that the oxygen removal in water did not have the same significance for the sparing effect at the FLASH irradiation dose rate (Boscolo et al., 2021).

In this thesis, irradiated targets consisting water, buffer, culture medium and lysed cells with various forms of irradiation were investigated using FLASH pulses laser-accelerated electrons with ultra-high dose rates and X-rays with conventional dose rates. Preliminary experiments were conducted in order to investigate and examine the ideal temperature probe, dosimetry and sample placement which were reported in Chapter IV. After finalizing the experimental setup, the measurement of oxygen removal in various samples irradiated with X-rays and laser-accelerated electrons was performed and presented in Chapter V.

## CHAPTER II

### BACKGROUND AND KNOWLEDGE

#### 2.1 Radiotherapy

Over the years, there have been many types of cancer treatments such as surgery, chemotherapy, immunotherapy and others used to treat patients. Each method is used in different cases, and in some patients more than one treatment may be required. Nonetheless, radiotherapy, also known as radiation therapy (RT), is one of the most popular cancer treatments today. RT directly uses ionizing radiation and also indirectly uses the radical molecules that are produced from the interactions in water radiolysis to damage the DNA. Cells' growth will be reduced as a result of these processes. Their DNA will not be repaired, and the cells will be destroyed. Currently, many external beams are used in cancer therapy, both conventional beams (photon beams) and ion beams, for example, protons and carbon ions. However, in this section, we will only discuss the x-ray and electron beams, which are beams used in this research.

##### 2.1.1 Electron and X-ray radiation

Radiation can be classified into two main processes consisting of non-ionizing and ionizing radiation (Bushberg et al., 2005). Non-ionizing radiation does not have the ability to ionize matter. In contrast, ionizing radiation can ionize matter through both direct and indirect ionization. For directly ionizing radiation, the energy from the ionizing charged particle can transfer to the medium via Coulomb interactions with the atom's orbital electrons. Charged particles such as electrons, protons, heavy ions and others are categorized as directly ionizing radiation. Indirect ionizing radiation is a type of radiation in which neutral particles such as photons and neutrons deposit their energy in the medium. At first, these neutral particles will release the charged particles in the medium and then these charged particles will interact with the orbital electrons of the atom in the medium. In this work, the physics of electron and X-ray radiation are

mentioned because these two particles were used in the experiments.

### Electron radiation

The incident electron could interact with the medium through Coulomb interactions with orbital electrons and atomic nuclei. The interaction between the incident electron and orbital electrons results in the excitation and ionization of the absorber atoms. The interaction between the incident electron and atomic nuclei leads to electron scattering and energy loss through the Bremsstrahlung process which is more prominent in the x-ray radiation. Loss of electron kinetic energy is described by stopping powers that are a combination of collision and radiative stopping powers arising from energy losses from electron-orbital electron and electron-nucleus interactions, respectively. The linear stopping power is determined in the form of the kinetic energy loss by an electron per unit of the path length ( $dE/dx$ ) (Bushberg et al., 2005). The mass stopping power is the linear stopping power divided by the density of the medium ( $\rho$ ) as evident in the equation 2.1. In the equation 2.2, the total mass stopping power is also the sum of the mass stopping powers from two interactions: electron-orbital electron  $(S/\rho)_{col}$  and electron-nucleus interactions  $(S/\rho)_{rad}$ .

$$(S/\rho)_{tot} = -\frac{1}{\rho} \frac{dE_k}{dx} \quad (2.1)$$

$$(S/\rho)_{tot} = (S/\rho)_{col} + (S/\rho)_{rad} \quad (2.2)$$

### X-ray radiation

X-ray radiation has been widely used in radiotherapy. When the electron hits the X-ray target, the kinetic energy of the electron is transferred to the target. Then the target excited and emitted X-ray photons. X-rays are separated into two groups consisting of characteristic X-rays and bremsstrahlung X-rays. Characteristic X-rays are called discrete X-rays. When the incident electron interacts with the inner electron of the target atom, the kinetic energy of the incident electron, which has more energy than the binding energy of an electron shell in a target atom, can kick the electron out of its shell, leading to a vacancy. Immediately, the outer shell electron moves to fill the vacancy and

then the characteristic X-ray is emitted with a unique energy equal to the difference of binding energies between the two shells (Bushberg et al., 2012). In part of the bremsstrahlung X-rays, the incident electron interacts with the nucleus, resulting in the deceleration and loss of kinetic energy of the incident electron and then the bremsstrahlung photons are produced by the radiation energy that is equal to the lost energy of electrons. When many electrons have the bremsstrahlung interaction, a spectrum of X-ray energies is produced. Accordingly, the X-rays from the bremsstrahlung process are sometimes called continuous X-rays. Then, these X-ray photons interact with the medium and release charged particles. Finally, these charged particles interact with the orbital electrons of the medium's atom through direct Coulomb interactions and deposit energy into the medium.

For no charged particles such as X-rays, the decreasing in a number of photons when photons pass through the matter is known as attenuation. The relation between the number of incident photons ( $N_0$ ) and the number of transmitted photons that remained without any interaction ( $N$ ) can be written as shown the equation 2.3. The total linear attenuation coefficient is the sum of each individual attenuation coefficient of interactions that can happen with the photon, consisting of the photoelectric effect ( $\mu_{\text{photoelectric effect}}$ ), coherent (Rayleigh) scattering ( $\mu_{\text{Rayleigh}}$ ), Compton scattering ( $\mu_{\text{Compton}}$ ) and pair production ( $\mu_{\text{pair production}}$ ) as shown the equation 2.4.

$$N = N_0 e^{-\mu x} \quad (2.3)$$

$$\mu = \mu_{\text{photoelectric effect}} + \mu_{\text{Rayleigh}} + \mu_{\text{Compton scatter}} + \mu_{\text{pair production}} \quad (2.4)$$

### 2.1.2 The absorbed dose

In radiotherapy, a physical quantity used to measure the energy deposited in tissues is defined as an absorbed dose. The absorbed dose ( $D$ ) is equal to the mean energy deposited by ionizing radiation per unit mass of medium (Allisy et al., 1993) with the special unit gray (Gy), where 1 Gy is equal to 1 J/kg (reports series, 2008). The calculation of the absorbed dose follows the equation below

$$D = \frac{d\epsilon}{dm} = \frac{1.6 \times 10^{-9}}{\rho} \times \frac{dE}{dx} \times F \quad (2.5)$$

where  $d\epsilon$  is the mean energy,  $dm$  is a medium's mass, and  $dE/dx$  is a stopping power (the energy loss of the particles per unit length) for mass density  $\rho$  that is deposited by a parallel beam with particle fluence  $F$  (Schardt et al., 2010).

### 2.1.3 Water radiolysis

Water radiolysis is a process that isolates water molecules by ionizing radiation. Generally, several situations, including food irradiation, radiosterilization and radiotherapy result in water radiolysis (Le Caër, 2011).

Ionizing radiation process can occur from particles (helium ions, electrons, protons, and neutrons) and electromagnetic (gamma rays and X-rays). Ionizing radiation causes a variety of ionic and excited states in water, which further break down or combine to produce radical and molecular species as shown in the equation 2.6. The mechanism of water radiolysis can be explained into 3 stages: the physical stage, the pre-chemical or physico-chemical stage and the chemical stage, depending on different typical time scales of irradiation. Starting with the physical stage, the production of electrons  $e^-$ , ionized  $H_2O^+$  and excited water  $H_2O^*$  molecules were occurred in  $10^{-15}$ s after the ionizing radiation interaction from ionization and excitation. During the pre-chemical stage ( $10^{-15}$ s -  $10^{-12}$ s), many radicals were produced from reactions such as dissociative relaxation, ion-molecule reaction and the production of hydrated electrons from autoionization of excited states and thermalization of subexcitation electrons. The final stage as the chemical stage is happened during the time scale of  $10^{-12}$ s -  $10^{-6}$ s. In this stage, the radicals can react with each other and other surrounding molecules and then diffuse into solution. The main reactions occurred during the mechanism of water radiolysis and the radical productions are summarized in the figure 2.1.

Chemical species from water radiolysis especially the hydroxyl radicals ( $OH^\bullet$ ), solvated electrons ( $e_{aq}^-$ ) and hydrogen radicals ( $H^\bullet$ ) can interact with DNA resulting in the DNA damage. Moreover, ( $e_{aq}^-$ ) and ( $H^\bullet$ ) can also react with the oxygen dissolved in the solution and then produce the toxic reactive species

such as superoxide ( $\text{O}_2^{\bullet-}$ ) and perhydroxyl radicals ( $\text{HO}_2^{\bullet}$ ).

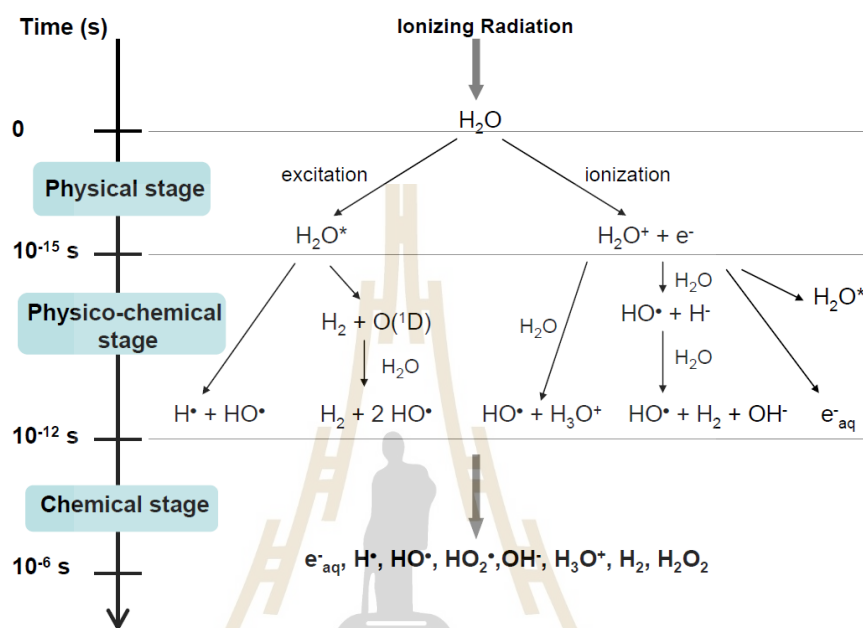
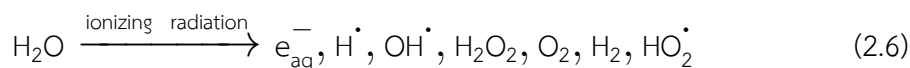


**Figure 2.1** The main reactions take place during water radiolysis. The different chemical radicals are generated in three main stages, consisting of the physical, physico-chemical and chemical stages, via different time scales (Le Caër, 2011).

## 2.2 Tumor Oxygenation

### 2.2.1 Oxygen transport to tissue

At the room temperature, oxygen is a colorless, odorless and tasteless gas. It's an important element for all living beings including humans, animals and plants. Approximately 21% of all gases in our atmosphere, oxygen is the second most abundant gas after nitrogen (Lareau and Fahy, 2020). Moreover, 90% of our biochemical and metabolic activities need oxygen.

In mammals, oxygen is drawn from the ambient air and carried to the tissues by the bloodstream of the circulatory system. Blood transports oxygen to tissues in two ways: (1) dissolved within red blood cells (RBC cells) and

plasma, accounting for approximately 2% of total oxygen, and (2) bound to hemoglobin, known as oxyhemoglobin, accounting for approximately 98% of total oxygen (Pittman, 2011). When oxyhemoglobin is formed in tissues, oxygen and hemoglobin are separated, resulting in an increase in the local partial pressure of oxygen ( $pO_2$ ) in that tissue. During cellular respiration, cells use oxygen to produce energy, which is then used for a wide range of cell activities.

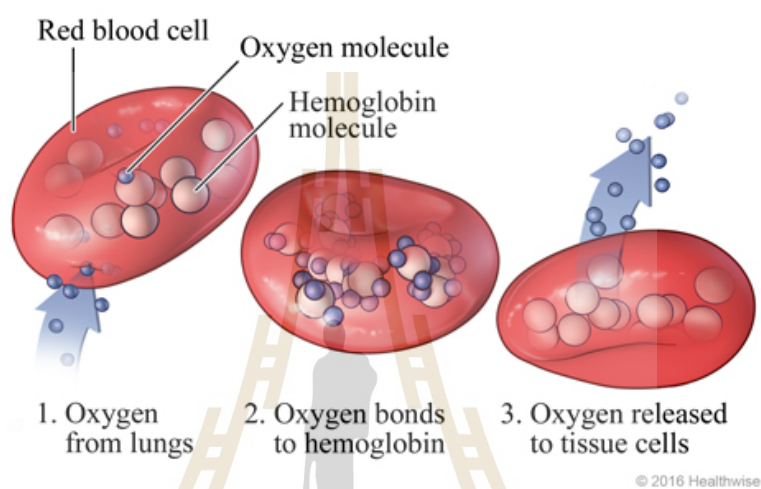


**Figure 2.2** Oxygen is transported to tissue cells by using the hemoglobin protein in the red blood cell (Staff, 2020).

### 2.2.2 Hypoxic tumors

Tumor is a group of abnormal cells that forms a solid mass of tissue as shown in figure 2.3. Tumor microenvironments have low oxygen areas. The condition in which tumor cells are oxygen-starved is called tumor hypoxia or hypoxic tumor as seen in figure 2.4. Normally, there is not much oxygen in the normal cells, usually about 5%. But for tumors, it is even less. The median oxygen is between 0.3% and 4.2% depending on the location and type of the cell (McKeown, 2014).

Hypoxic tumors are a major issue in cancer treatment. Compared to healthy cells, tumor cells proliferate and increase more quickly. Deeply located cells cannot get enough oxygen from the blood vessels, which leads to hypoxia. The lower oxygen level in the hypoxic tumor cells exhibits and is associated with a poor outcome of the cancer treatment because these tumor cells are radio

resistance. In contrast to the normal cells that are radiosensitive, free radicals will be produced after the irradiation and they will interact with the oxygen molecules in cells. These new radicals cause damage to DNA, resulting in the destruction or death of cells. However, hypoxia could reduce the efficiency of cell damage. Tumor cells irradiated using X-rays in two different oxygen levels revealed that the radiosensitivity of the cells was approximately three times greater in a well-oxygenated condition than those of in a hypoxic condition (Gray et al., 1953). With this result, researchers have faced great challenges in developing radiation techniques to address the hypoxia problem of tumor cells (Muz et al., 2015).

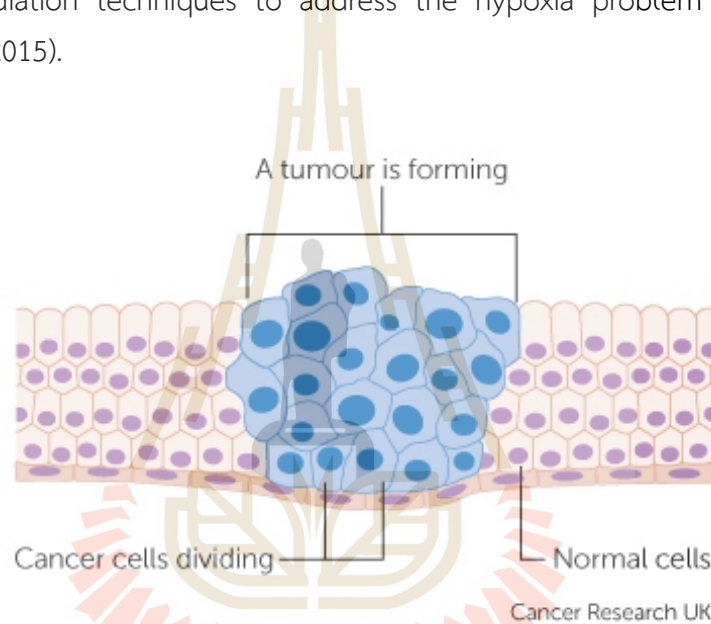


**Figure 2.3** A bunch of cancer cells spreads out to nearby normal cells (Cancer Research UK, 2020).

### 2.3 FLASH irradiation

Radiotherapy is widely used for many cancer patients' treatments. Nonetheless, conventional radiotherapy (CONV-RT) still has some limitations on the maximum tolerated dose for normal tissues. The conventional dose is usually around 2 Gy per fraction or less (Omyan et al., 2020). With this dose, not only normal cells but also tumor cells are given time to recover from the potentially harmful effects of irradiation. Therefore, there is a critical need to improve and develop RT to find a new strategy that can help to spare

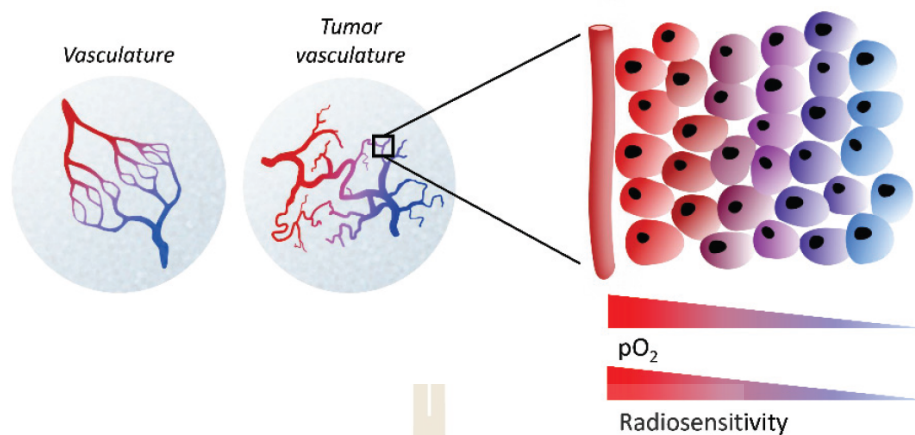


**Figure 2.4** The abnormal growth of tumor cells is the result of inadequate transport of oxygen molecules from blood vessel to cells. Cells that are very distant from the blood vessels do not receive enough oxygen and increasing the hypoxia regions. Hypoxic cells are one problem for the radiotherapy treatment because they are irradiation resistance (Ramachandran et al., 2015).

normal tissue while increasing the tumor-destroying effect of RT. One of the new treatments has been developed by managing on the frame time of the irradiation, which is known as “FLASH irradiation”.

FLASH radiotherapy (FLASH-RT) has become widely attractive in the past ten years due to advances in increasing normal tissue sparing in the radiation. In nature, the word “flash” comes from lightning, which can strike in a very short amount of time while holding a very high energy discharge. FLASH refers to ultrashort in radiation medicine, which is the delivery of a high treatment dose in sub-second timescales for one-time irradiation (GSI Helmholtz Centre for Heavy-Ion Research GmbH, 2021). FLASH-RT uses the ultra-high dose rate of 40 Gy/s which is higher than the dose rate used in CONV-RT (around 0.03 Gy/s). With the different dose rates between both radiotherapy methods, FLASH-RT has an advantage in terms of the treatment time which will be faster than CONV-RT, if compared with the same total treatment doses. Furthermore, the studies consistently demonstrated that normal tissues were protected by FLASH irradiation were better than by conventional irradiation. FLASH irradiation provide an alternative mean to kill tumor tissues with a higher dose.

In fact, some scientists have been researching ultra-high dose experiments since the 1950s-1990s, but the term “FLASH” irradiation was first used in 2014. There was a study of the different responses between normal and tumor tissues of mice lungs that were irradiated with ultra-high dose rate (FLASH) and CONV irradiation (Favaudon et al., 2014). Compared to the CONV, the FLASH irradiation showed a decrease in normal tissue toxicities, which is known as the “FLASH effect”.

### 2.3.1 FLASH effect

As mentioned in the previous section, FLASH irradiation has the advantage of sparing normal tissues. Many *in vitro* and *in vivo* experimental models have been investigated. In the 1970s, normal mice were irradiated using 7 MeV electrons at different dose rates while breathing oxygen. The experimental result showed a decrease in the radiation sensitivity in tissues when the dose rate was higher than 60 Gy/min (Hornsey and Bewley, 1971). Some time later, the experimental study on rat skin had been performed with a radiation dose rate of 500 Gy/min (Field and Bewley, 1974). The results showed that the ultra-high dose rate caused more adverse effects than the low dose rate for irradiation in aerobic conditions. Furthermore, neither experiment demonstrated a change in radiation sensitivity from anoxic irradiation. In 2014, FLASH irradiation received more attention again in which the experiment in the lung C57BL/6 mice. Mice were exposed to CONV-RT (0.03 Gy,  $\gamma$ -rays or 4.5 MeV electrons) or FLASH-RT (60 Gy/s, 4.5 MeV electrons) with 17 Gy of the radiation dose for comparing between two different irradiation (Favaudon et al., 2014). After 24 weeks of irradiation, mice irradiated with CONV-RT developed dense fibrosis, whereas mice irradiated with FLASH-RT developed no lesions. However, fibrosis was observed in FLASH-RT but with the delivery dose increased to 30 Gy after 24 weeks of irradiation. The investigation on larger animals had been conducted in addition to the experiment on small animals such as mice. The mini-pig was irradiated on both sides of its back. Radiation doses in the range of 22–34 Gy were delivered with a CONV dose rate (0.083 Gy/s) on one side of the back and a FLASH dose rate (300 Gy/s) on another side of the back. The irradiated skin was observed for 36 weeks after radiotherapy (Vozenin et al., 2019). At this point, the CONV-irradiated skin had depilation and skin fibronecrosis in all areas

of irradiation, whereas the FLASH-irradiated skin had only minor depilation and the skin's pigment changing in the irradiated area as shown in figure 2.5.

The sparing effect in the normal tissues is not only one reason that FLASH-RT has gained attention worldwide but its effectiveness in tumor control after the irradiation is also one of the important aspects of FLASH-RT that have been considered in their studies. FLASH irradiation was as effective as CONV irradiation in controlling tumor cell growth in human breast tumor (HBCx-12A) and head-and-neck carcinoma cells (HEp-2). As part of the same research on the mini pig skin, there were six cat patients with squamous cell carcinoma (SCC) of the nasal planum. Cats were irradiated with FLASH electrons in a single dose ranging from 25–41 Gy. After the irradiation, only three cats showed some depilation without acute/late side effects, and the other three had only mild or moderate symptoms of mucositis/dermatitis with no toxicity. Moreover, the tumor was permanently controlled in five out of 6 cats after 16 months. Only one cat showed a recurrence of SCC after 21 weeks. The picture of the cat patient (cat no. 2) before and after the treatment is shown in figure 2.6.

Interestingly, in 2019, the first human patient with T-cell cutaneous lymphoma was interested in and agreed to engage with FLASH-RT (Bourhis et al., 2019). A 3.5 cm tumor on his right forearm was treated by FLASH-RT with 15 Gy in 90 ms. The tumor began to diminish starting from 10 days and finally, the tumor response was complete 36 days after the irradiation. For the normal tissues surrounding the lesions, redness, and mild epithelitis were observed during 10-44 days after the irradiation. A good result from this treatment was continually updated for 5 months later. The pictures of the tumor before and after treatment are shown in figure 2.7. However, FLASH-RT treatment is still considered limited, the mechanism and factors for FLASH-RT have yet to be confirmed. Thus, FLASH research is constantly being developed in order to obtain higher experimental data for clinical application.

### **2.3.2 Oxygenation and oxygen depletion**

Although FLASH irradiation has shown satisfactory results in many studies but the mechanism behind FLASH has not yet been adequately described. Many experiments were repeated in order to determine the mechanism of FLASH. Currently, one of the most extensive explanations for the FLASH mechanism is

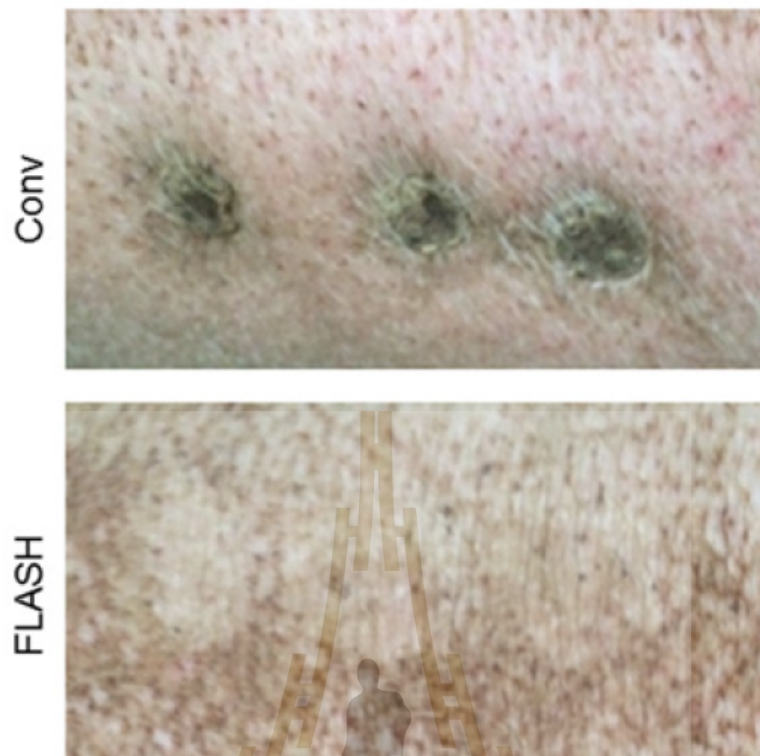


**Figure 2.5** A microscopic visualization of mini pig skin, thirty-six weeks after radiotherapy. Images above and below are the irradiation effects on mini pig skin following CONV-RT and FLASH-RT, respectively. Three spots are yielded from three different delivery doses, which are 34, 31 and 28 Gy from the left to the right spot, respectively. The irradiated skin with CONV dose rates shows fibronectic lesions. Whereas in the irradiated skin with the FLASH dose rate, there are only a few depilations and pigmentations. (Vozenin et al., 2019).

the oxygen depletion hypothesis.

In 1958, the experimental study of the sensitivity to radiation in *Shigella flexneri* bacteria with a shot-pulsed irradiation of 1.2 MeV electron beams showed that the sensitivity of the bacteria changed depending on the oxygenation level before the irradiation. Furthermore, the findings confirmed that oxygen could diffuse into or out of the bacteria in a short period of time, but under anoxic conditions (in a pure nitrogen gas environment). The biological effect did not increase when the bacteria were given oxygen after the microsecond irradiation (Howard-Flanders and Moore, 1958). Later, *Serratia marcescens* bacteria were



**Figure 2.6** A microscopic visualization of the lesion on the cat patient (cat no. 2). The advanced squamous cell carcinoma (SCC) of the nasal planum before the irradiation (A). After 14 months of FLASH irradiation (B), the tumor lesions were gone and didn't have mucositis and skin erythema (Vozenin et al., 2019).

irradiated with X-rays at dose rates of 0.1 Gy/s and with electron beams that can deliver a dose of 100-200 Gy in 2  $\mu$ s. The result showed the higher survivor bacteria or the decreasing of the sensitivity in the oxygenation condition with the ultra-high dose rate irradiation (Dewey, 1959). The studies at the time sparked interest in ultra-high dose rate irradiation research. Furthermore, early research in bacteria cells exposed to ultra-high dose rates resulted in the breaking survival curves shown in figure 2.8. The break-point dose is defined as the absorbed dose that caused the irradiated cells to be in an anoxic environment, causing the slope of the survival curve to change. The radiochemical depletion of oxygen during irradiation caused the mechanism of breaks at ultra-high dose rates.

In addition to the experiment in bacteria, the studies in mammalian cells are also considered. In the ultrahigh dose rate experiment with HeLa S-3 cells, the cell responsibility measured in 0% and 21% oxygen show the similar effect as in the conventional irradiation. While in the survival curves of very low oxygen concentrations, the break-points are represented in the curves (Epp et al., 1972). However, *in vitro* studies in mammalian cells have not confirmed the FLASH effect, and the current study has both the presence and



**Figure 2.7** The progress of a tumor lesion on the human arm before and after treatment: (A) a lesion of T-cell cutaneous lymphoma with a tumor size of 3.5 cm before treatment. (B) At 3 weeks after treatment, a critical reaction on the skin surrounding the tumor with redness and asymptomatic mild epithelitis. (C) The tumor responded perfectly and was strong for the following 5 months (Bourhis et al., 2019).

absence of this phenomenon (Hughes and Parsons, 2020). Normal tissues in general FLASH experiment of *in vivo* studies may have an oxygen tension of 3-7%. But cells cultured in an air-conditioned environment have an oxygenation level of approximately 20%. Therefore, the FLASH studies in these *in vitro* experiments did not have enough significance to reduce the oxygen tension during the irradiation. In 2020, the ultrahigh dose rate experiment with prostate cancer cells showed the cells at oxygen concentrations of 1.6–4.4% are more resistant compared to that of the CONV-RT at the same dose of irradiation (Adrian et al., 2019). In comparison to cells at concentrations greater than 8.3%, there is no difference between CONV and FLASH irradiation as shown in figure 2.9. The recent simulation in oxygenated water with the computational model did not show the sparing effect in the FLASH dose rates (Boscolo et al., 2021). Therefore, the impact of oxygen depletion on FLASH irradiation must be experimentally investigated more thoroughly.

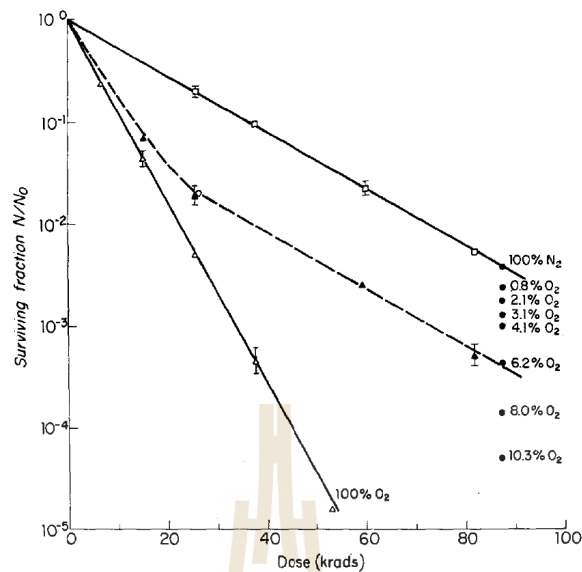


**Figure 2.8** A graph shows the relationship between the adsorbed dose (horizontal axis) and the surviving fraction (vertical axis). *E.coli B/r* bacteria were irradiated using a single 3 nanosecond pulse of ultra-high dose rate irradiation for cells equilibrated at 23 °C. At a dose of approximately 25 krads, the breaking survival curve was produced in the line for 6.2 percent oxygen concentration (Weiss et al., 1974).

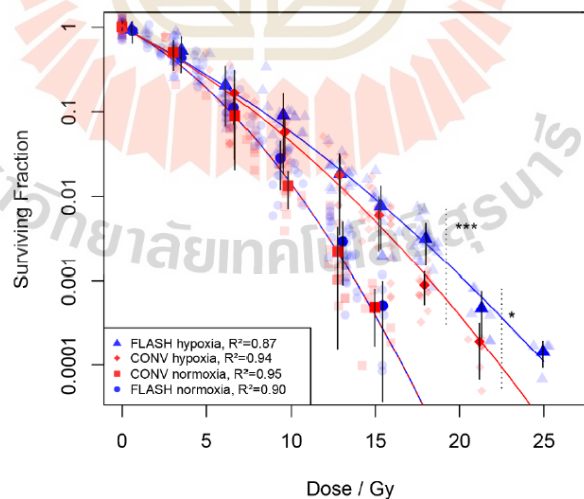


**Figure 2.9** The survival fraction of prostate cancer cells was determined by the difference in irradiation doses under normoxic (20% oxygen concentration) and hypoxic (1.6% oxygen concentration) conditions. When doses were increased in hypoxic cells, the surviving fraction from FLASH irradiation (blue line) was clearly higher than that from CONV irradiation (red line) (Adrian et al., 2019).

## CHAPTER III

### MATERIAL AND METHODS

This chapter presents the equipment used and various processes in oxygen measurement. The sample container, sample preparation and experiment setups had been separated into two types for the suitability of the experiment. Two different beams with different dose rates had been used in this study. X-ray beams were used for low dose rate experiment and an accelerated electron beam was used for ultra-high dose rate experiment. Details of measurement principles are also explained in this chapter as well.

#### 3.1 Instruments for oxygen measurement

In this study, almost all the equipment used for the oxygen measurement is from PreSens Precision Sensing GmbH, Germany. There are three main components comprising an oxygen meter, accessories and sensors. The OXY-1 SMA-RS232-AO is a compact fiber optic oxygen meter as shown in the figure 3.1. The oxygen meter has temperature correction which allows to obtain the most accurate measurements in temperature-changing situations. The oxygen meter is connected with a polymer optical fiber (POF) that has a wide-range oxygen sensitive coating or PSt3. The excitation light is transferred to the sensor and the sensor's response is transferred back to the meter via the POF. This excitation light is generated from the LED inside the oxygen meter at a wavelength of 505 nm. The chemical optical oxygen sensors SP-PSt3-SA23-D5-OIW-US with a diameter of 5 mm were used to measure the oxygen concentration with a time resolution of 1 s. The sensors have self-adhesive technology and can be attached to the surface of a glass or plastic vessel. For monitoring and collecting the oxygen concentration, the oxygen meter has been operated using PreSens.EOM STS software.



**Figure 3.1** A compact fiber oxygen meter OXY-1-SMA-trace-RS232-AO (PreSens Precision Sensing GmbH, 2015)

### 3.1.1 The measurement principle

The measurement for detecting oxygen is based on the luminescence quenching principle by oxygen molecules, which is a quencher in general. After the optical fiber transfers the excited light from the oxygen meter to the spot sensor, the luminophore in the sensor absorbs that light to increase the energy level from the singlet ground state ( $S_0$ ) to the excited electronic singlet state ( $S_1$ ), as shown in the Jablonski diagram (Figure 3.2). The singlet state ( $S_1$ ) can be de-excited by the intersystem crossing and drives it to an excited triplet state ( $T_1$ ). In order to return to the singlet ground state, the luminophore in the singlet excited state emits short-lived light known as fluorescence (Ast et al., 2012). Whereas in the excited triplet state, the luminophore returns to its original ground state by long lived emission or phosphorescence. Since the oxygen molecule's ground state is a triplet ground state ( $^3O_2$ ), the luminophore in the excited triplet state is extremely efficient at interacting with the oxygen molecule. After collision, energy from the luminophore is transferred to the oxygen molecule, resulting in the change in the states of oxygen molecule by changing from the ground state to its excited state ( $^1O_2$ ). As a result, the excited indicator molecules no longer emit light, reducing the overall luminescence lifetime. Collisional quenching reduces the luminescence lifetime ( $T$ ) of the luminophore depending on an oxygen concentration. The quenching

behavior is described in the Stern-Volmer equation (PreSens Precision Sensing GmbH, nd):

$$\frac{\tau_0}{\tau} = 1 + K_{SV} \cdot [O_2] \quad (3.1)$$

$\tau$  is luminescence decay time in presence of oxygen

$\tau_0$  is luminescence decay time in absence of oxygen

$K_{SV}$  is Stern-Volmer constant

And  $[O_2]$  is oxygen concentration.

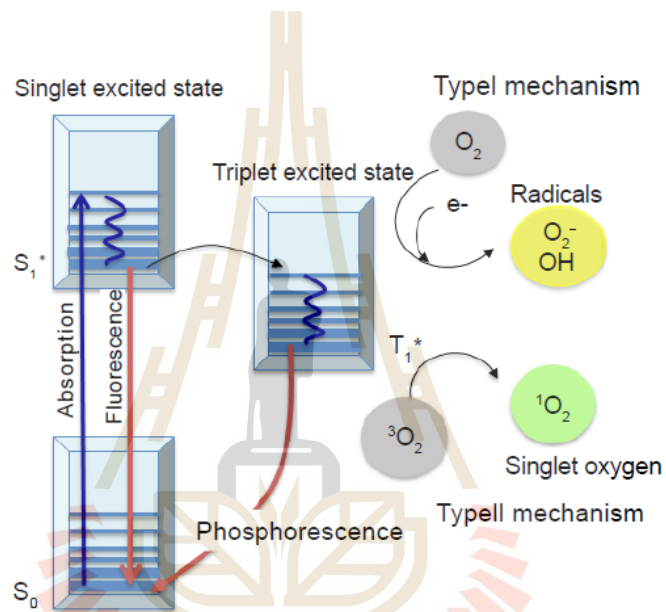


**Figure 3.2** Jablonski diagram describes the possible state of the indicator molecule (phosphore). The triplet excited states of the luminophore can interact with the oxygen molecule by electron transfer, generating radical species (Type I mechanism) or energy transfer to the oxygen molecule, changing the state of oxygen (Type II mechanism) (Alemany Ribes et al., 2013).

### 3.1.2 Container setups

Since there are two different parts of the experiments: low-dose rate irradiation with the X-ray beam and ultra-high dose rate irradiation with electron experiments, the sample containers were designed into two different configurations suitable for each experiment.

Figure 3.3 shows the container used for X-ray irradiation. It is made up of four main parts: an empty plastic container, an inset, a rubber stopper and a spot sensor. The spot sensor was glued on one side to the inner wall of the empty plastic container in the center between the container and the inset. The inset was formed to fit the empty container in a similar shape and to have the empty area for liquid samples. One side of the inset is opened for the oxygen measurement. It is attached against the wall of the empty container that has a spot sensor. To have an area for containing the sample, the inset and the container are firmly glued together with silicone rubber glue. There is a circular hole at the top of the inset used to fill the liquid sample. Next, the rubber stopper is used to seal the sample area, keeping the sample gas-tight and preventing oxygen from diffusing in. The pre-assembled container will be able to contain a liquid sample of approximately  $1 \text{ cm}^3$  in volume. A small plastic connection is affixed to the outer surface of the container, in the same position as the spot sensor, with a small fitting hole for connecting the fiber optic cable for measuring oxygen in the sample.

The container used in laser-accelerated electron irradiation is shown in figure 3.4. The complete container is made up of three cylindrical parts. These three parts have different functions and are attached together to provide a suitable container for the experiment. The first part is the middle part which is a one-open-end cylindrical container with a 5 mm inner diameter and a 5 mm depth. The open end is covered with a thin piece of transparent plastic with a spot sensor in the center. This side is glued to the second part, a part with a hole for holding the optical fiber cable. The bottom of the container has a tiny hole for filling the container with the sample using a needle. This side is sealed and glued with a third part that has a spiral hole for connecting a screw and holds the container the proper position. Both inset pieces for X-ray irradiation and the cylindrical container for electron irradiation were produced at GSI using polyetheretherketone (PEEK) material to avoid radiation intelligence or chemical leaching. PEEK is a semicrystalline linear aromatic polymer that is usually recognized as the top performing thermoplastic material with excellent hydrolysis resistance. Moreover, the crucial point is that it is radiation- and chemically resistant and does not release oxygen into the sample when irradiated.

### 3.1.3 Samples preparation

Full oxygenated water, deoxygenated water, phosphate buffered saline (PBS), culture medium (Ham's F12) and lysed cells are used as samples in this study. All samples preparation were handled differently according to sample types and containers. For ready-made samples such as full oxygenated water, PBS and culture medium, there is no special preparation required. Thus, we can fill them directly into containers (under clean conditions). In contrast, more preparation steps are required for other samples such as deoxygenated water and lysed cells. To prepare deoxygenated water, a laboratory bottle was filled with full oxygenated water and progressively added nitrogen gas to reduce the oxygen level in the liquid for 10-15 minutes. For the lysed cells, a confluent T-75 flask of LM8 (Osteosarcoma) cells was trypsinated, centrifuged and resuspended in a 0.1 g/ml suspension in PBS. Cells were sonicated in a bioruptor sonicator 18 times in 30 s, and the complete disruption of nearly all cells was confirmed under the microscope. For both experiments, X-ray irradiation and laser-accelerated electron irradiation, it is important to check air bubbles that may occur during or after the container is filled with the sample. For the container in the X-ray irradiation, the container was gently tapped in order to help dislodge any visible air bubbles before sealing the sample area with a rubber stopper. For laser-accelerated electron irradiation experiments, after filling the container with sample, sample is injected again with a syringe. If there are any air bubbles, they will come out with the sample overflowing through the sample injection channel. Finally, the container is sealed completely using the remaining cylindrical parts.

## 3.2 Sensor calibration

Sensor calibration is an important step in any measurement. Although the oxygen measurement has default constants that are predetermined for the measurement by the manufacturer, oxygen sensor spots still have to be calibrated before using in the experimental condition for reliability and accuracy. A traditional two-point calibration must be performed in an oxygen-free environment and air-saturated.

The first calibration point is oxygen-free water. It is labeled as Cal 0.

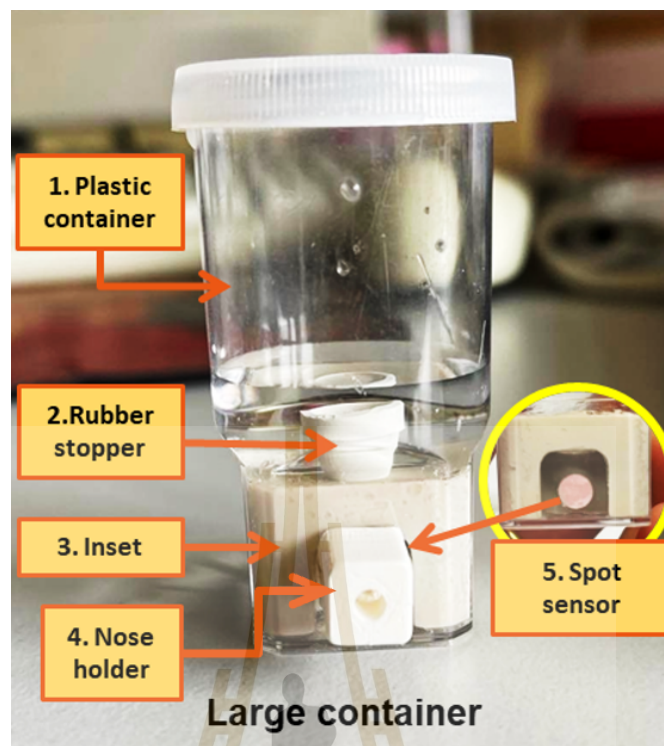


**Figure 3.3** A container was filled with the sample for X-ray irradiation. A spot sensor was installed in the container's wall. A nose holder was affixed to the container on the outside to hold the optical cable in the same place as the spot sensor. For the sample, a PEEK inset was bonded to the container's wall with a hole on top for a rubber stopper to maintain a steady oxygen concentration.

To make the calibration standard Cal 0, 1 g of sodium sulfite ( $\text{Na}_2\text{SO}_3$ ) was dissolved in 100 ml of water. The reaction between oxygen and  $\text{Na}_2\text{SO}_3$  produces oxygen-free water as  $\text{Na}_2\text{SO}_3$  is used to remove oxygen that diffuses from air into the water. Next, bottle filled with solution was shaken for approximately one minute to ensure that the water is oxygen free. The solution was poured into the containers as in the sample preparation process so that the calibration is in similar condition to the actual experiment. Next, the second calibration point is water vapor-saturated air which is used as a calibration standard, Cal 100. For calibration with a container for X-ray irradiation, the wet cotton was placed on top and the channel is closed to fill the liquid sample. For calibration with a container for laser-accelerated electron irradiation, the wet cotton was placed

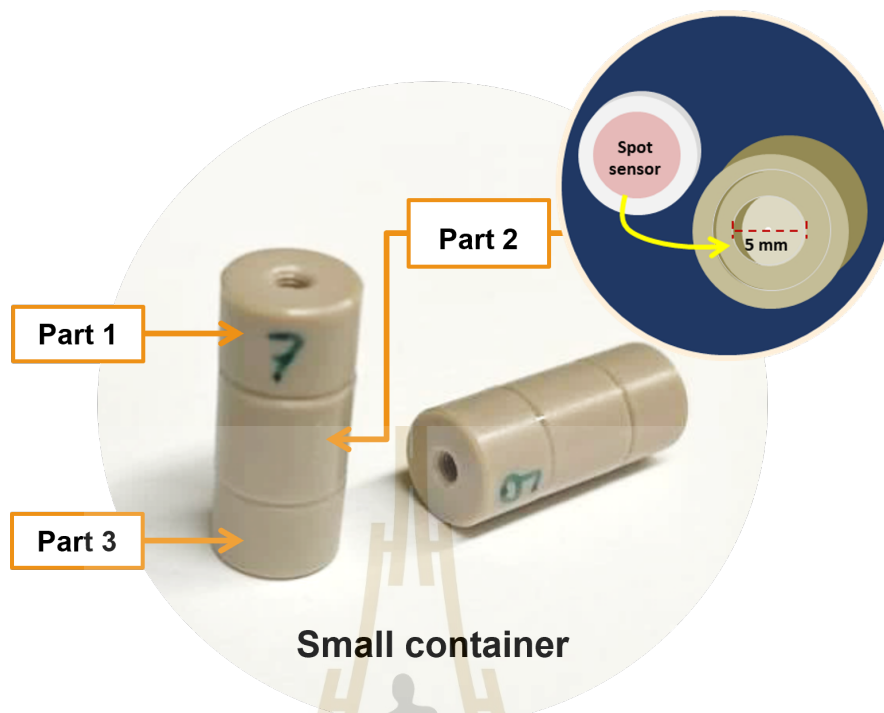


**Figure 3.4** Samples for electron irradiation using the PHELIX laser and some experiments with X-ray irradiation were contained in a cylindrical container with inner dimensions of 5 mm x 5 mm. The spot sensor was positioned on the lid of the container. The optical fiber holder was fastened to the top of the container. A small hole in the bottom of the container was used for injecting samples and was glued with the screw holder.

in an empty bottle. The container was added with a small amount of water and was placed in the same bottle near the wet cotton. In order to ensure the air inside container is water vapor-saturated, leave the container around 2 minutes and then, start the calibration afterwards.

### 3.3 Irradiation modalities

Two separate beams were used to investigate the oxygen removal in irradiated samples at two different dose rates; low and ultra-high dose rates. The low dose rate irradiation comes from a 250 kV photon X-ray system. Meanwhile the ultra-high dose rate employed MeV electron beams generated by the PHELIX-laser with an electron energy of  $> 7$  MeV for the ultra-high dose

rate irradiations. Both irradiations were carried out at Darmstadt, Germany's GSI Helmholtz Centre for Heavy-Ion Research GmbH.

### 3.3.1 PHELIX laser

The Petawatt High-Energy Laser for Heavy Ion Experiments (PHELIX) is one of the largest lasers in Germany. It is a laser facility capable of producing powerful laser beams with energies of up to 1 kJ in 10 ns for long pulse mode and 200 J in 20 ps for short pulse mode. It has been used to investigate a variety of studies, the majority of which are linked to plasma and atomic physics. Figure 3.5 shows the target chamber for intense laser experiment in the PHELIX experiment area. Electrons were produced and accelerated by the interaction of laser pulses of relativistic intensities with foam targets of near critical density (NCD). The foam target in this study is the low-density polymer foam layer, triacetate cellulose (TAC,  $C_{12}H_{16}O_8$ ). A high number of electrons are generated by an effective mechanism called direct laser acceleration (DLA) (Zähler, 2020).

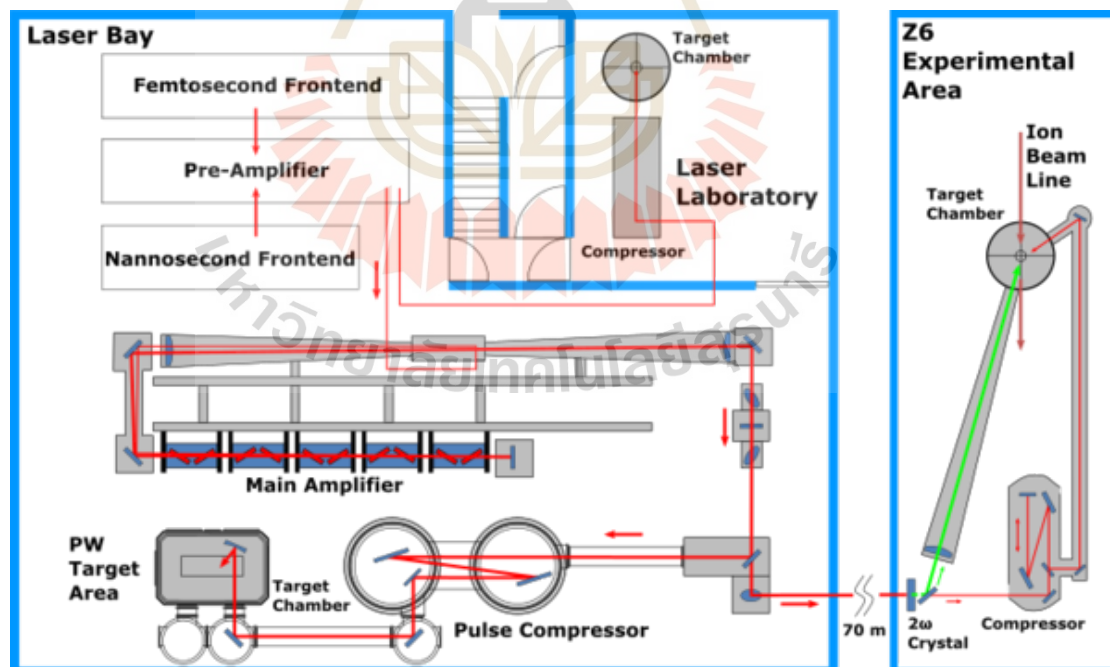


**Figure 3.5** The experiment area of PHELIX laser building at GSI Helmholtz Centre for Heavy-Ion Research (GSI Helmholtz Centre for Heavy-Ion Research GmbH, nd).

## 3.4 Experimental Setup and Dosimetry

### 3.4.1 X-ray irradiation setup

In X-ray irradiation, samples were placed in both types of containers. Full oxygenated water, deoxygenated water and PBS buffer samples were filled into the large container (figure 3.3) at a volume of approximately  $1 \text{ cm}^3$ . Culture medium, lysed cells and some PBS buffer samples were put into the small vacuum tight containers as in the section 3.1.2. The samples were irradiated at the center below the X-ray target and the Semiflex ionization chamber (IC, type number TM31013, PTW, Germany) was placed beside the sample operating as a dosimetry of the X-ray irradiation as shown in figure 3.6. In addition, these samples were irradiated at different dose rates depending on the containers. The dose rate for the large container was between 4.5 and 4.8 Gy/min, while the dose rate for the tiny container was between 10.0 and 10.4 Gy/min.

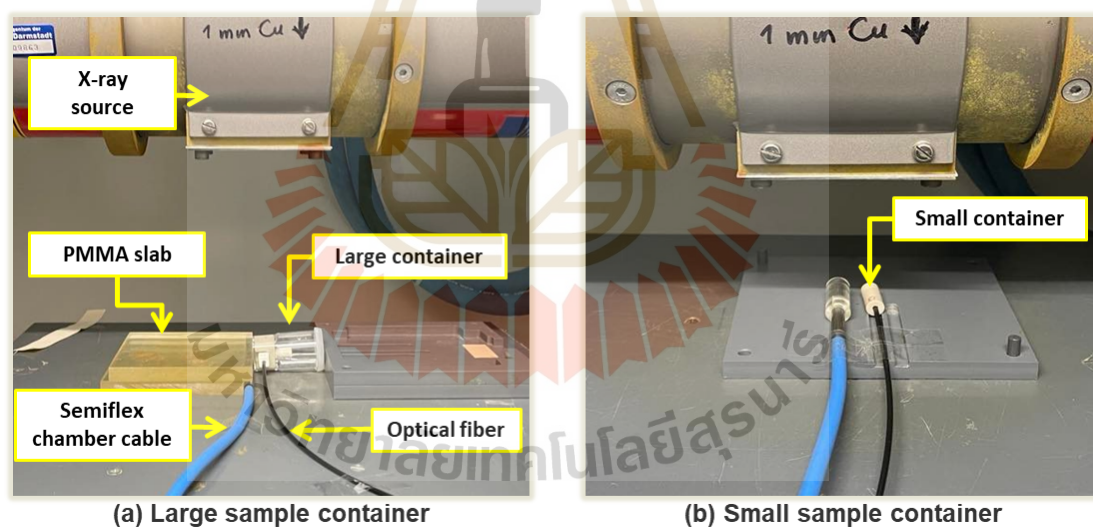


**Figure 3.6** Experimental setup for X-ray irradiation in irradiated samples in the large container (left) and the small container (right). The dosimeter was placed beside the containers under the PMMA slab for the large container or inside the chamber lid for the small container.

### 3.4.2 Laser-accelerated electron irradiation setup

For irradiation using the PHELIX laser, all samples were filled into small containers except for deoxygenated water which was handled the same way as in the X-ray irradiation. The sample is attached to the mounting device in a direction parallel to the direction of the laser. In this irradiation, XD radiochromic films (RCFs) and TLD cards are used as dosimetry to measure the dose provided at various distances in front of and behind the sample as shown in figure 3.7. This setup is placed in the target chamber. Two optical fiber cables were used: the first cable in the target chamber is used for sending the signal from the sample to the second cable via a feedthrough and then the second cable forwards the signal back to the oxygen meter. To evade the electromagnetic radiation coming from the external environment during the irradiation, the oxygen meter and laptop are kept in a Faraday cage. Due to the setup, the results cannot be observed in real-time thus another laptop which was connected wirelessly to the laptop in the control room was used to control the display screen and observe the measurement results. Figure 3.7 (a), (b) show mini-RCFs placed inside the container to measure the dose inside the container for some shots. The dose rate is roughly 30 Gy in 20 ps. Two XD-RCF sheets were positioned behind the foam target to absorb the produced short-range proton component.

### 3.4.3 Dosimetry

Radiation dosimeters are devices or systems that measure various values of ionizing radiation. There are many types of dosimetry, but in this study, we focused on the ionization chamber, radiochromic film and thermoluminescent dosimeter (TLD).

#### Ionization chamber

The ionization chamber measures the dose and dose rate of X-ray irradiation. The basic structure of an ionizing chamber is a gas volume between two electrodes coupled to a high voltage source. When irradiated, the ion pairs consisting of positive and negative charges are created in this gas volume. Then the electrodes receive these charges and create a current that can be

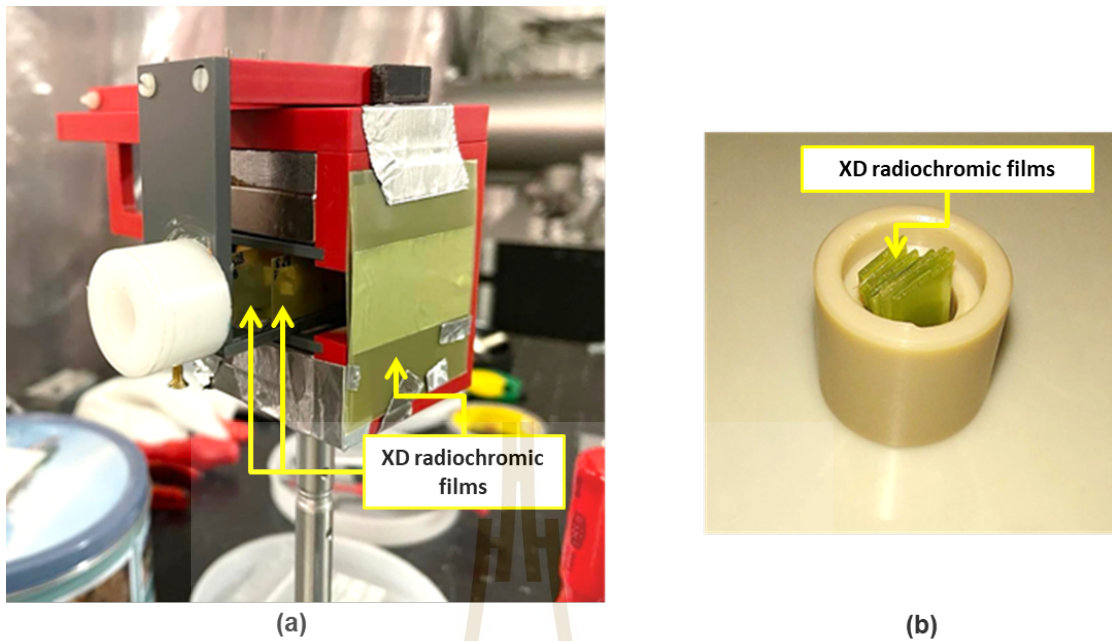


**Figure 3.7** Experimental setup used for laser-accelerated electron irradiation. A sample was placed between XD-RCF sheets, and a TLD card was placed behind this setup. Both the XD-RCF sheets and the TLD card were used as the dosimetry. To absorb the proton component, two large XD-RCF sheets were employed (a). Mini-RCFs were employed to measure the dose inside container (b).

measured by an electrometer. The absorbed dose in air ( $D_{\text{air}}$ ) is defined as:

$$D_{\text{air}} = \frac{Q}{m_{\text{air}}} \left( \frac{W_{\text{air}}}{e} \right) \quad (3.2)$$

where  $m_{\text{air}}$  is air mass,  $Q$  is ionization charge,  $W_{\text{air}}$  is the average energy expanded in the air per ion pair and  $e$  is the electron charge (Bushberg et al., 2005). The mean energy required to produce an ion pair in dry air or  $W_{\text{air}}/e$  is 33.97 eV/ion pair or 33.97 J/C. To determine the absorbed dose at a point in the medium (usual water)  $D_w$ , the subsequent conversion of the air cavity dose  $D_{\text{air}}$  to medium  $D_w$  is based on the Bragg-Gray or Spencer-Attix cavity theories.  $D_w$  is proportional to the mean absorbed dose in the detector  $\bar{D}_{\text{air}}$  with the ratio of the mass stopping powers water to air  $S_{w,\text{air}}$  which can be described

as:

$$D_w = D_{\text{air}} \cdot S_{w,\text{air}} \quad (3.3)$$

### Radiochromic films

Radiochromic films (RCFs) are composed of two main layers: radiation-sensitive material layers and a thin polyester base with coating. These dosimeters are based on the property of ionizing radiation to alter the structural characteristics of their crystalline sensitive elements. The interaction of ionizing radiation with the film produces a polymerization process in the layer of the radiation-sensitive material which changes the film's color. The darkening of the film is related to the radiation dose.

### Thermoluminescent dosimeters

Thermoluminescent dosimeters (TLDs) are based upon the formation of a metastable crystalline structure with valence electrons to absorb and store the energy of ionizing radiation. The valence electron is excited by the ionizing radiation. The electron travels through a solid state in a conducting band for a short time and then drops into the trap of a gap between the conduction and valence bands. When heated, the electrons escape from the trap and return to the valence band with the emission of light and we call this light thermoluminescence or TL.

## CHAPTER IV

### PRELIMINARY TEST

In this chapter, two dosimeters were used for the dosimetry test. Full oxygenated water and PBS samples were irradiated with the X-ray in different directions of sample containers. Finally, oxygen removal in irradiated samples was kept as the preliminary result of the experiment.

#### 4.1 Dosimetry Test

Ionization chambers and dosimeters have played a crucial role in experimental studies related to irradiation. The factors influencing radiation measurement vary across different experiments, and these variations can be attributed to either the type of dosimeter used or the amount associated with the radiation field.(INTERNATIONAL ATOMIC ENERGY AGENCY, 2001).

The Semiflex ionization chamber (IC, type number TM31013, PTW, Germany) is a conventional dosimeter that is used in the X-ray machine in this experiment. But the sample area is small. Therefore, another dosimeter as the Pinpoint chamber (type number TM31009, PTW, Germany) is used to do the dosimetry test in this experiment with the advantage that the Pinpoint ionization chamber is smaller and gives superior spatial precision inside the radiation field than the Semiflex ionizing chamber. A dosimetry test has been performed to verify the accuracy of the Pinpoint ionization chamber. In this test, two parameters consisting of the dosimeter and the dosimeter's position were defined as influence qualities that affect the dosimetry.

The first part of the dosimetry test started with a sensitivity comparison between the Pinpoint ionization chamber and the Semiflex ionization chamber. The radiation doses were measured under the same conditions and at the same irradiation time. The Pinpoint ionization chamber was placed under the PMMA (Polymethyl Methacrylate) slabs and measured the radiation dose for two minutes. Then, the Pinpoint ionization chamber was replaced by the Semiflex ionization chamber and it was irradiated for two minutes. There were three

repetitions with the same dosimeter and setup to find the average value of the radiation dose. The experimental setup revealed discrepancies in the measured radiation doses when utilizing different dosimeters. Thus, the dosimeter becomes a significant factor in dosimetry. To compensate for the disparities between the Pinpoint ionization chamber and the Semiflex ionization chamber, a correction factor is required when quantifying radiation dose. The correction factor of the dosimetric factor ( $C_d$ ) was determined as the ratio between doses given from the Semiflex ionization chamber and the Pinpoint ionization chamber under the same condition of irradiation (see equation 4.2.).

The next influential parameter is the dosimeter's position. Directly measuring the irradiation dose at the sample's position is not feasible. Consequently, dosimetry near the sample area in different positions was deemed essential. The dosimetry was separated into two sections consisting of the dosimetry where the Pinpoint ionization chamber was placed under the slabs and under the container. First, the pinpoint ionization chamber was placed below the slabs. The irradiation was carried out for two minutes. There were three repetitions for each irradiation setup. Next, the dosimeter was placed in a different position to measure the doses by placing it under the container below the sample area. The sample was irradiated for two minutes and repeated three times. The layout of the container is divided into two directions: horizontal and upright. Following the measurement, the results revealed that the given doses differed depending on the position of the dosimeter. Therefore, the dosimeter's positions were another quality that affected the dosimetry. The correction factor of geometry ( $C_g$ ) was described as the ratio of given doses when the dosimeter was placed beside the container and under the container (see equation 4.3).

The real dose that the pinpoint dosimeter received was corrected from the relation between the measured dose and the correction factor as shown in the equation 4.1. Moreover, the correction factors were differently defined depending on the positions of the dosimeter (beside or below the container) and the directions for container placement (an upright or horizontal direction).

$$\text{Real dose} = \text{Displayed dose} \times C_d \times C_g \quad (4.1)$$

$$C_d = \left( \frac{\text{Received dose from Semiflex}}{\text{Received dose from PinPoint}} \right) \quad (4.2)$$

$$C_g = \left( \frac{\text{Received dose under the PMMA slab}}{\text{Received dose under the sample container}} \right) \quad (4.3)$$

**Table 4.1** List of correction factors according to the position of container and dosimeter during irradiation.

container's position	Dosimeter's position			
	Under container		Beside container	
	$C_d$	$C_g$	$C_d$	$C_g$
Upright	0.717	1.202	0.730	1
Horizontal	0.730	1.287		

## 4.2 Preliminary results

In this particular section, preliminary experiments involved the utilization of easily prepared samples, consisting of fully oxygenated water and PBS, for X-ray irradiation. The samples were exposed to 2-3 irradiation steps, with a dose rate ranging from 4.2 to 4.9 Gy/min, with the Pinpoint ionization chamber serving as the dosimeter. Depending on the correction factor as described in Section 4.1, the samples received an actual dose of 50 to 66 Gy in a single irradiation step. The graph illustrating the removal of oxygen during the irradiation process is presented in figure 4.1. In this particular section, preliminary experiments involved the utilization of easily prepared samples, consisting of fully oxygenated water and PBS, for X-ray irradiation. The samples were exposed to 2-3 irradiation steps, with a dose rate ranging from 4.2 to 4.9 Gy/min, with the Pinpoint ionization chamber serving as the dosimeter. Depending on the correction factor as described in Section 4.1, the samples received an actual dose of 50 to 66 Gy in a single irradiation step. The graph illustrating the

removal of oxygen during the irradiation process is presented in figure 4.1. The results show the maximum value of the oxygen removal was measured in the first step of irradiation and then the oxygen concentration was decreased in the next step or when the cumulative doses were increasing, varies according to different setups. Only in the PBS studies, where the container is upright and the PinPoint chamber is positioned beneath it, the average oxygen removal in the second step is slightly greater than the first measurement (first step), increasing from  $18 \mu\text{M}/\text{Gy}$  to  $19 \mu\text{M}/\text{Gy}$ , as shown in table 4.2.

Finally, the Semiflex chamber was used for the dosimetry in the final irradiation setup because the PinPoint chamber was unsuccessful in the orthovoltage energy range (at voltages of 150-500 kV) (Medina et al., 2008). The final experimental setup was performed by placing the sample container in the horizontal direction and having the dosimeter beside the sample container as mentioned in Section 3.4.1.

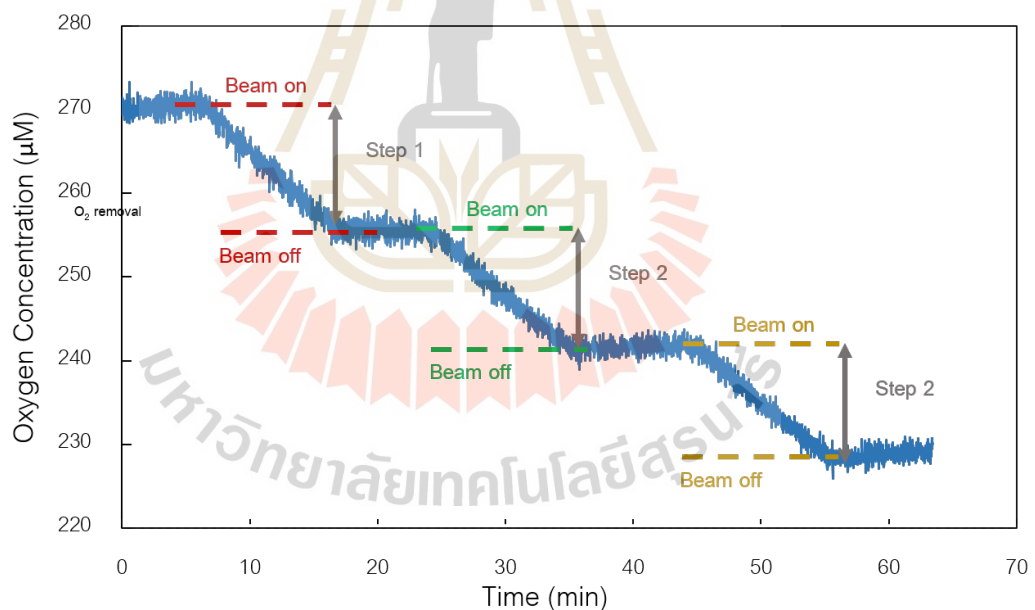
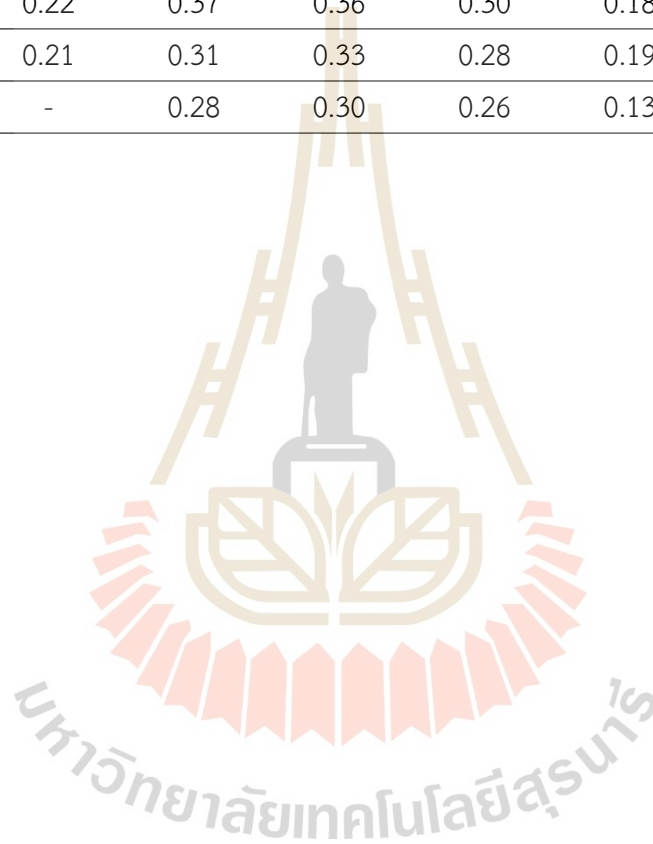


**Figure 4.1** A preliminary result from X-ray irradiation where a container filled with a water sample is placed in the horizontal direction and the PinPoint chamber is placed beside the container. The sample was irradiated for 3 steps at 51 Gy/step at a dose rate of 4.75 Gy/min.

**Table 4.2** The average oxygen removal in different setups depends on the container's direction and the dosimeter's position after X-ray irradiation

Step	Average oxygen removal [ $\mu\text{M}/\text{Gy}$ ]					
	Water				PBS	
	Sample-Upright		Sample-Horizontal		Sample -Upright	Sample -Horizontal
	IC-Under	IC-Beside	IC-Under	IC-Beside	IC-Under	IC-Under
1	0.22	0.37	0.36	0.30	0.18	0.28
2	0.21	0.31	0.33	0.28	0.19	0.23
3	-	0.28	0.30	0.26	0.13	0.22



## CHAPTER V

### RESULTS

#### 5.1 Oxygen removal in X-ray irradiation

In the experiment, the average oxygen concentrations before irradiation were found to be highest in PBS, with a value of 290.46  $\mu\text{M}$ . Subsequently, the concentrations decreased to 283.87  $\mu\text{M}$ , 224.22  $\mu\text{M}$ , 207.42  $\mu\text{M}$  and 180.54  $\mu\text{M}$  in full oxygenated water, cell culture medium, deoxygenated water, and lysed cells, respectively. Different samples were subjected to X-ray irradiation at various low dose rates, ranging from 4.5 Gy/min to 10.4 Gy/min. The irradiation process involved 2 to 3 steps, with each step delivering a dose of 50 Gy. Following each irradiation step, the beam was turned off for approximately five minutes before proceeding to the next step. Examples of oxygen removal curves during irradiation can be seen in figures 5.1-5.5. The presented curves depict the variations in oxygen concentration over time throughout the experiment. Notably, the oxygen concentration decreased during the beam-on periods while remaining constant during the beam-off periods. To provide a summary of the results, the irradiation experiment was repeated several times, and the values of oxygen removal per irradiated dose from all repetitions were compared with the cumulative dose. These comparisons are illustrated in figures 5.6 to 5.9. Finally, the data on oxygen removal were averaged based on the irradiation steps.

The average values of the removed oxygen are summarized in figure 5.10 and tables 5.1-5.5. The results reveal that the amount of oxygen removal was highest during the first irradiation step and then decreased in subsequent steps. For full oxygenated water, the average oxygen removal per dose in the first three steps was measured at 0.28, 0.25 and 0.23  $\mu\text{M}/\text{Gy}$ . In the case of deoxygenated water, the average oxygen removal per dose was observed as 0.26, 0.22 and 0.18  $\mu\text{M}/\text{Gy}$  respectively. Moving on to the biochemical samples, in PBS, the average oxygen removal per dose was 0.26  $\mu\text{M}/\text{Gy}$  in the first step, followed by values close to full oxygenated water, namely 0.26 and 0.23  $\mu\text{M}/\text{Gy}$  in the second and third steps of irradiation, respectively. When comparing all

sample types quantitatively, the average oxygen removal per dose for irradiated cell culture medium samples consistently remained the highest across all steps, measuring at 0.42, 0.38 and 0.37  $\mu\text{M}/\text{Gy}$  in the first, second and third steps, respectively. Finally, for lysed cells, the average oxygen removal in the first and second irradiation steps displayed similar values of 0.27  $\mu\text{M}/\text{Gy}$ .

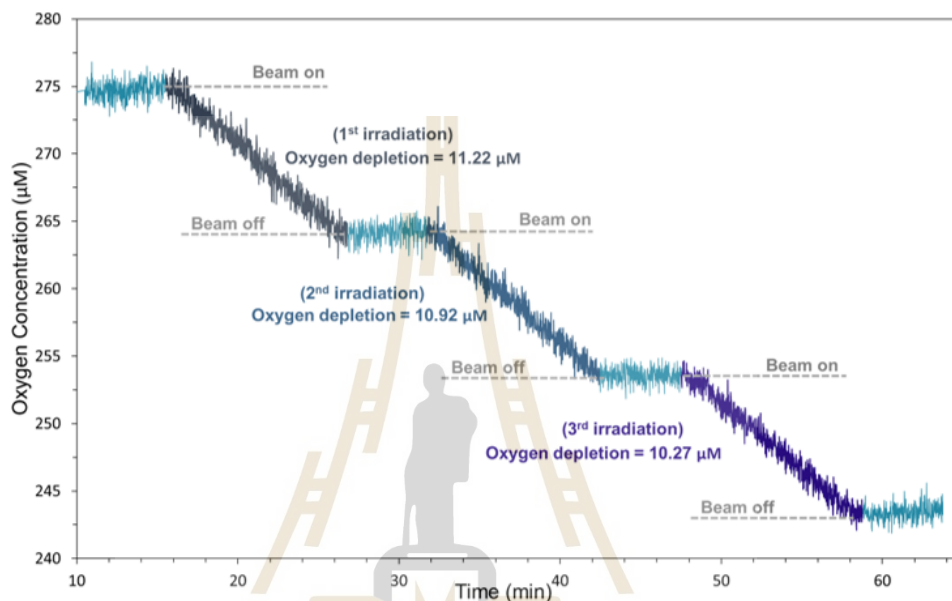


**Figure 5.1** An example graph of the oxygen concentration during three steps of X-ray irradiation in full oxygenated water. A sample was irradiated with a dose of 50 Gy/step.

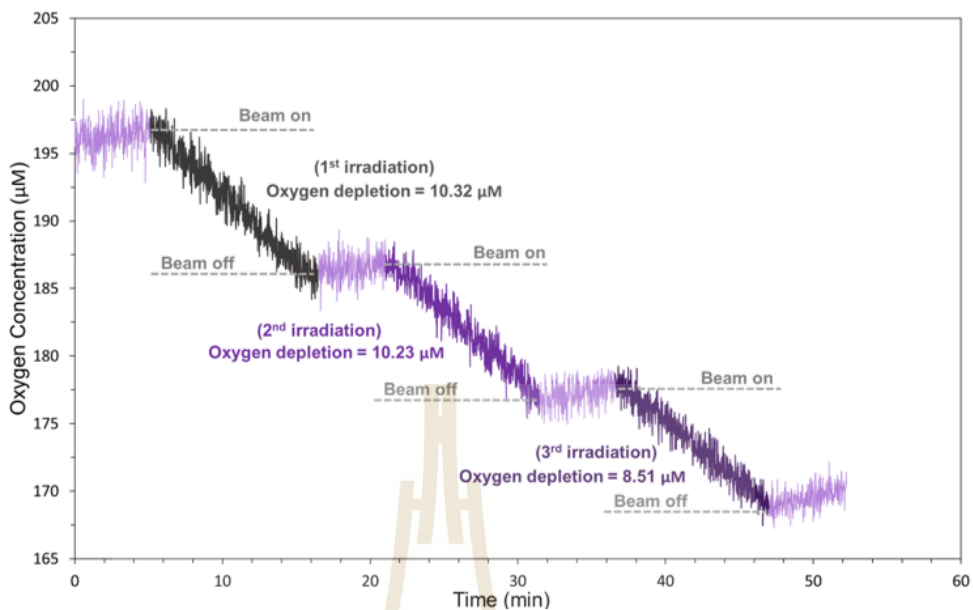


**Figure 5.2** An example graph of the oxygen concentration during three steps of X-ray irradiation in deoxygenated water. A sample was irradiated with a dose of 50 Gy/step.

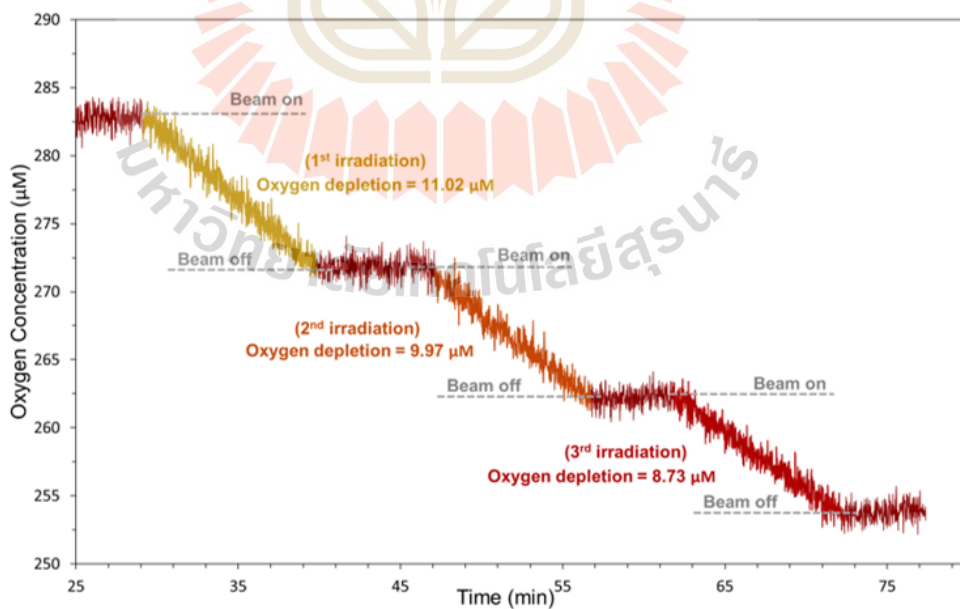


**Figure 5.3** An example graph of the oxygen concentration during three steps of X-ray irradiation in PBS. A sample was irradiated with a dose of 50 Gy/step.

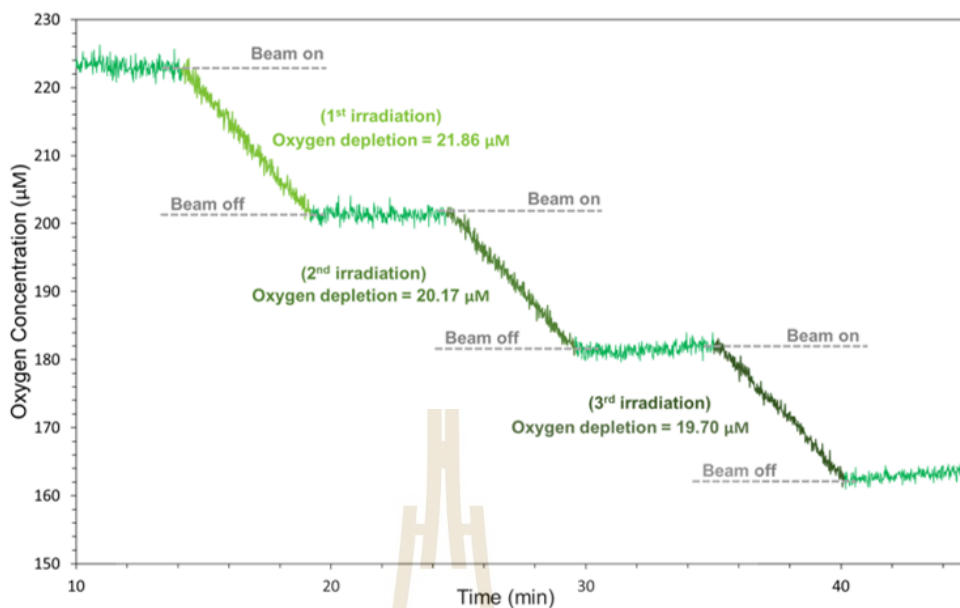


**Figure 5.4** An example graph of the oxygen concentration during three steps of X-ray irradiation in cell culture medium. A sample was irradiated with a dose of 50 Gy/step.

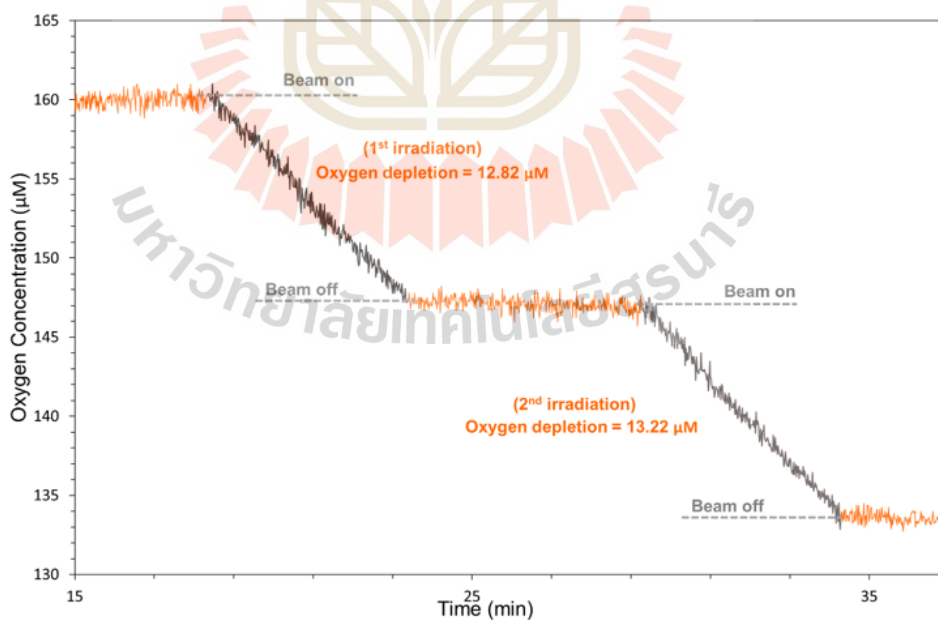
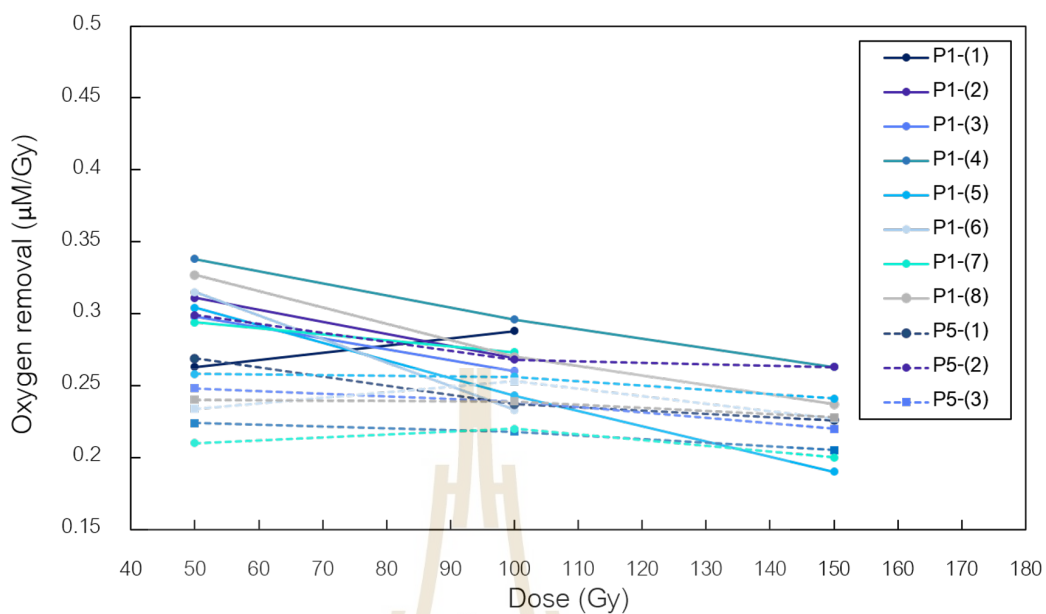
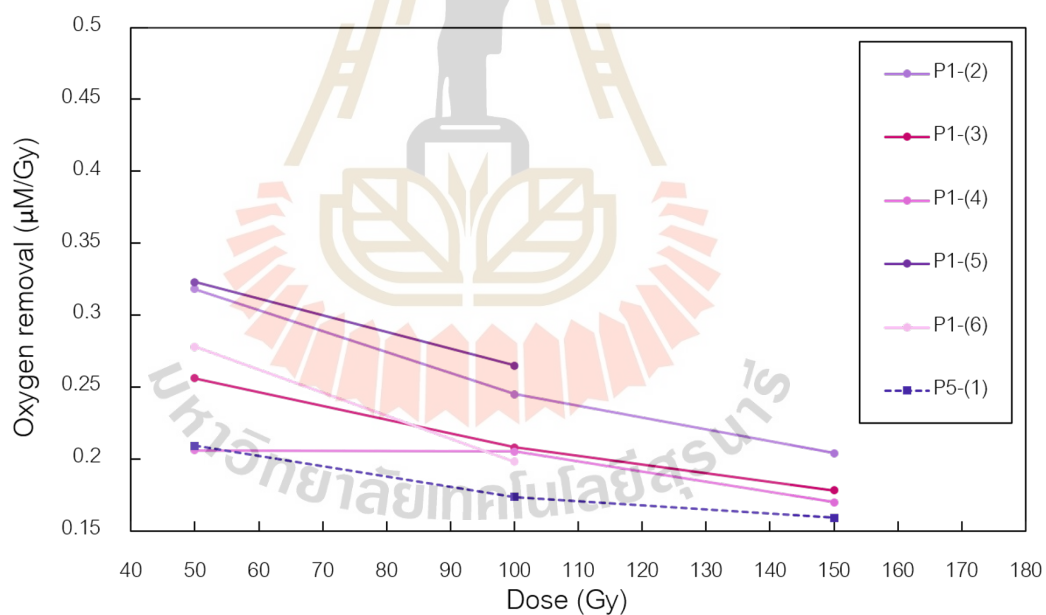


**Figure 5.5** An example graph of the oxygen concentration during two steps of X-ray irradiation in lysed cells. A sample was irradiated with a dose of 50 Gy/step.



(a)



(b)

**Figure 5.6** The oxygen removal per dose in each irradiation step of (a) full oxygenated water and (b) deoxygenated water. Different lines represent experiments using different containers. Solid and dotted lines represent the irradiation in samples contained in containers P1 and P5, respectively.

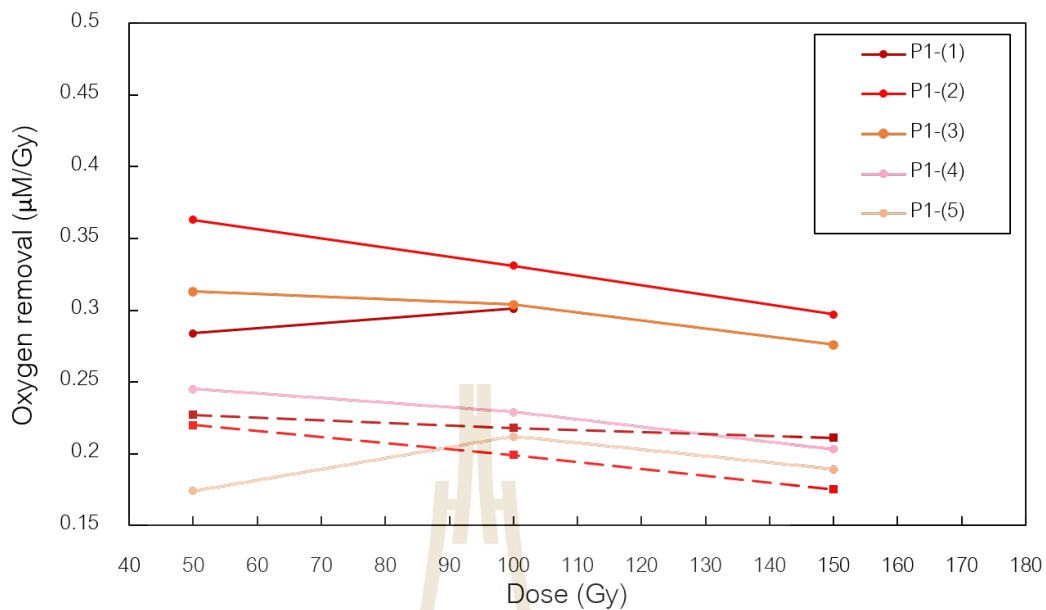


**Figure 5.7** The oxygen removal per dose of irradiated PBS samples compared to the given dose. The experimental results are from the large containers P1 and P5.

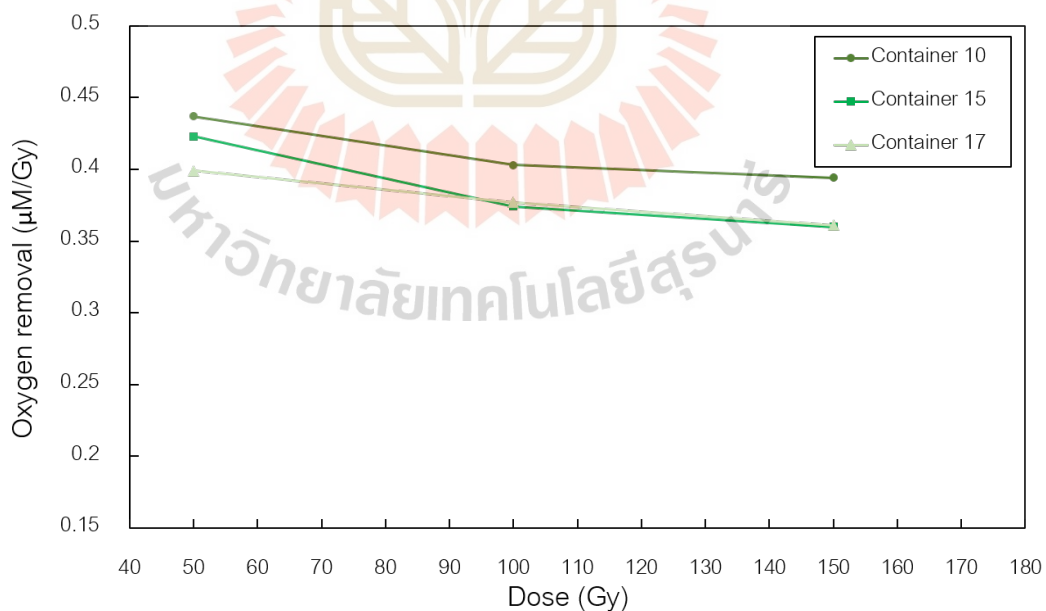


**Figure 5.8** The oxygen removal per dose of irradiated cell culture medium samples compared to the given dose. The cell culture medium results are from the container number 10, 15 and 17.

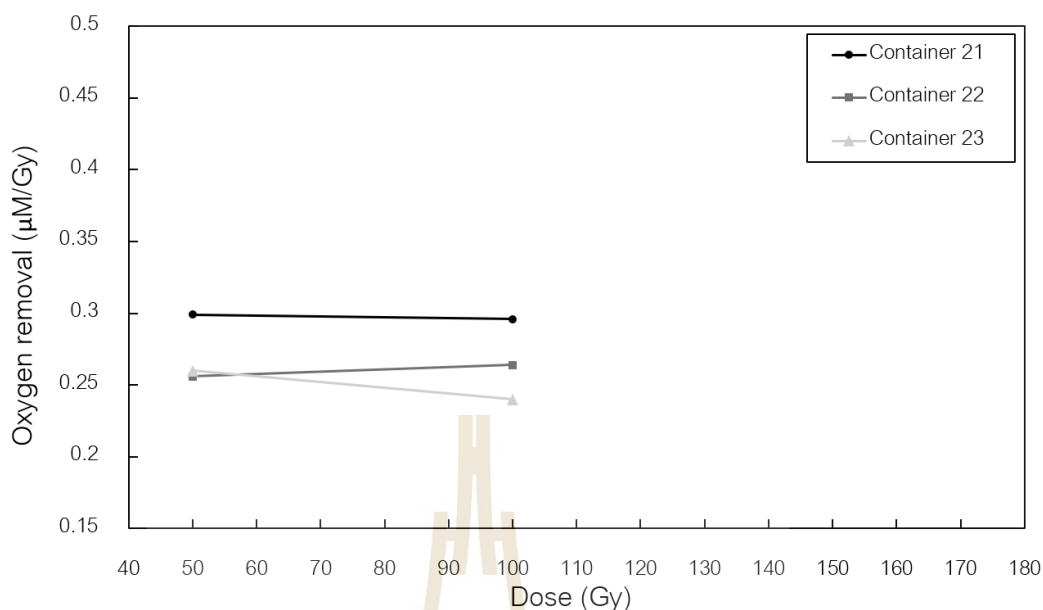


**Figure 5.9** The oxygen removal per dose of irradiated lysed cell samples compared to the given dose. The lysed cells results are from the container number 21, 22 and 23 respectively.

Furthermore, additional experiments were conducted where the beam resting time was extended to approximately two to five hours after the initial irradiation, followed by the second irradiation. The results of these experiments are depicted in figure 5.11 and table 5.6. In the second irradiation step, there was observed variation in the oxygen removal per dose, with some values higher, some equal, and some lower than the oxygen removal per dose in the first step. However, when considering the values presented in table 5.6, the average oxygen removal in the second step was found to be similar to that of the first step, with a value of  $0.27 \mu\text{M}/\text{Gy}$ .

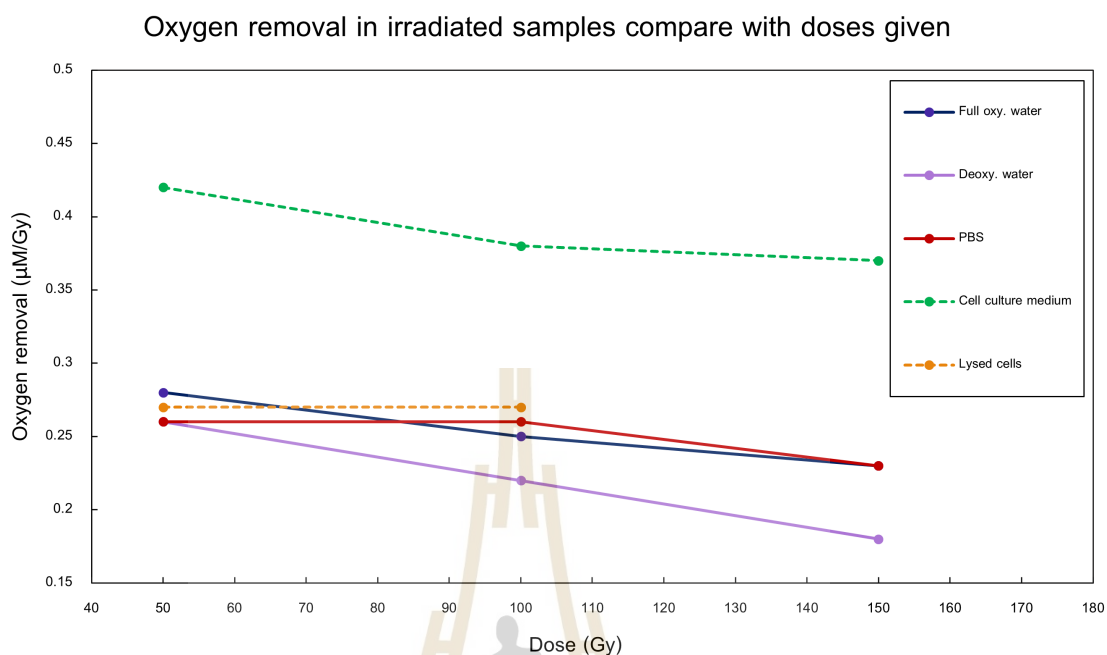


**Figure 5.10** The graph compares cumulative doses with the average oxygen removal across all sample types. Each line in the graph represents two to three points. The first point indicates the average oxygen removal in the samples after a radiation exposure of 50 Gy. The second and third points correspond to the average oxygen removal during the second and third irradiation steps, respectively.

**Table 5.1** The average oxygen removal per dose of full oxygenated water that received doses of 50 Gy per step. These average values were obtained from a total of 43 single data values (steps).

Step	Cumulative doses [Gy]	Average oxygen removal	Standard deviation
		[µM/Gy]	
<b>Full oxygenated water</b>			
1	50	0.28	0.039
2	100	0.25	0.023
3	150	0.23	0.024

**Table 5.2** The average oxygen removal per dose of Deoxygenated water that received doses of 50 Gy per step. These average values were obtained from a total of 17 single data values (steps).

Step	Cumulative doses [Gy]	Average oxygen removal	Standard deviation
		[ $\mu\text{M}/\text{Gy}$ ]	
Deoxygenated water			
1	50	0.26	0.048
2	100	0.22	0.033
3	150	0.18	0.019

**Table 5.3** The average oxygen removal per dose of irradiated PBS samples in large container that received doses of 50 Gy per step. These average values were obtained from a total of 20 single data values (steps).

Step	Cumulative doses [Gy]	Average oxygen removal	Standard deviation
		[ $\mu\text{M}/\text{Gy}$ ]	
PBS			
1	50	0.26	0.064
2	100	0.26	0.054
3	150	0.23	0.050

**Table 5.4** The average oxygen removal per dose of irradiated culture medium samples that received doses of 50 Gy per step. These average values were obtained from a total of 9 single data values (steps).

Step	Cumulative doses [Gy]	Average oxygen removal	Standard deviation
		[ $\mu\text{M}/\text{Gy}$ ]	
Culture medium			
1	50	0.42	0.019
2	100	0.38	0.016
3	150	0.37	0.019

**Table 5.5** The average oxygen removal per dose of irradiated lysed cells samples that received doses of 50 Gy per step. These average values were obtained from a total of 6 single data values (steps).

Step	Cumulative doses [Gy]	Average oxygen removal	Standard deviation
		[ $\mu\text{M}/\text{Gy}$ ]	
Lysed cells			
1	50	0.27	0.024
2	100	0.27	0.028

**Table 5.6** The average oxygen removal per dose of irradiated full oxygenated water samples that received doses of 50 Gy per step. After the irradiation in the first step, the experiment is in the rest periods (~1-5 hr) before the irradiation in second step. These average values were obtained from a total of 16 single data values (steps).

Step	Cumulative doses [Gy]	Average oxygen removal	Standard deviation
		[ $\mu\text{M}/\text{Gy}$ ]	
Full oxygenated water			
1	50	0.27	0.061
2	100	0.27	0.033

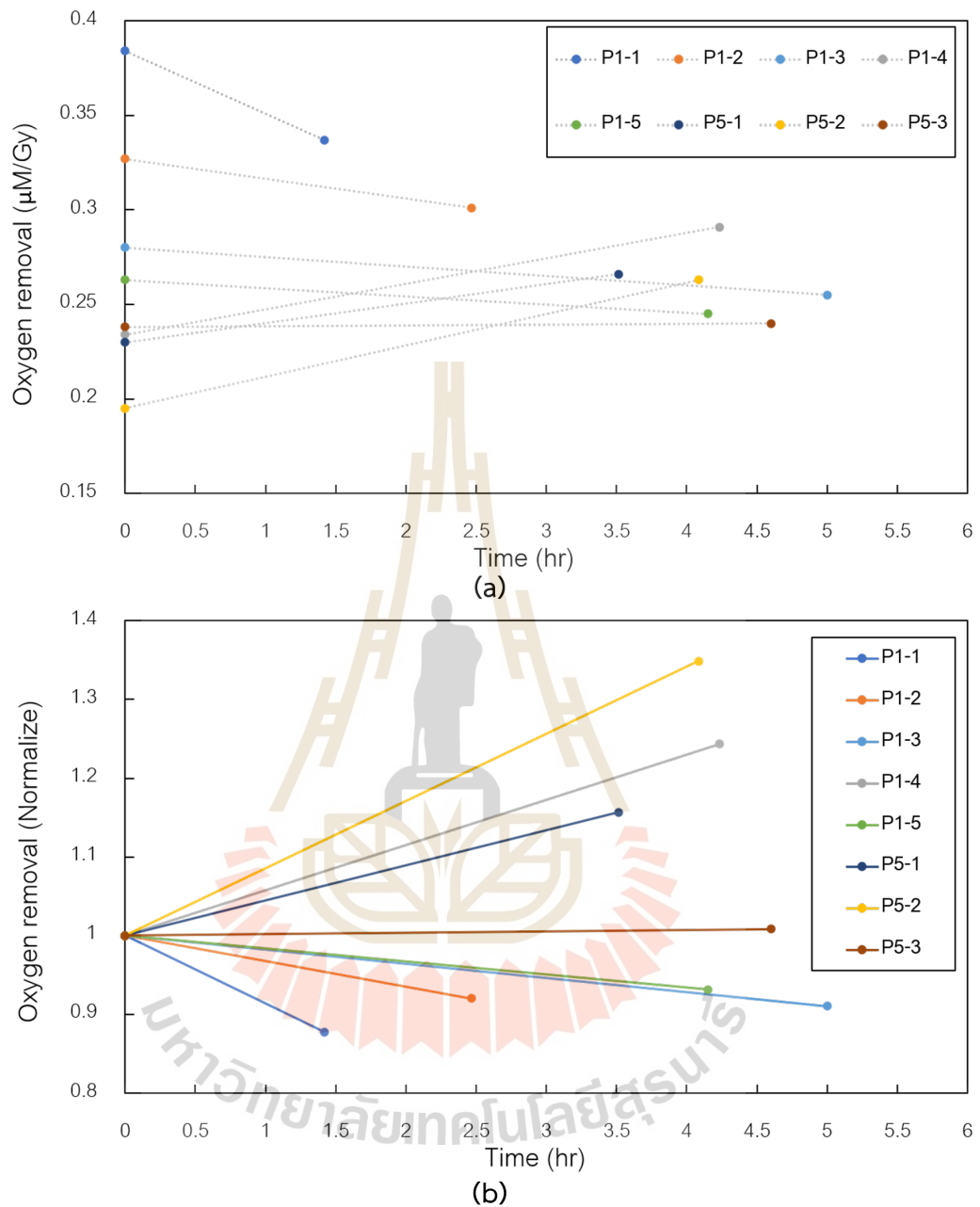


**Figure 5.11** The oxygen removal per dose in irradiated water samples compared to irradiated time. The first point on each line reflects the oxygen removal in the first step, which is always in time = 0 s. The second time point is when the irradiation in the second step begins after the beam has been turned off for an extended period of time ( $\sim 1$ –5 hours). (a) The results are based on the amount of oxygen removed per dose. (b) The oxygen removal in the first step results in normalization.

## 5.2 The irradiated samples from the PHELIX laser-accelerated electrons

Experiments at higher dose rates employing accelerated electrons from the PHELIX laser have been performed. Samples were irradiated for approximately 20 ps per shot. The overall number of experiments for irradiation was 32 shots, including 5 beam references, 5 dosimetry experiments, 4 coumarin experiments and 18 sample irradiations. This study was focused on the results of irradiated samples. Among those 18 irradiations, there are 4 shots for water, 4 shots for PBS, 5 shots for cell culture medium and 5 shots for lysed cells. The curves of all samples show the constant value of the oxygen level before the irradiation, then instantaneously drop in a short frame time during the irradiation and finally return to another constant level that is lower than the beginning (see figures 5.12-5.13).

Due to the complicated process of calculating the given doses for each shot, the average oxygen removal in each sample group was analyzed and summarized in figures 5.14 - 5.15 and table 5.7. The cell culture medium sample showed the minimum oxygen removal with a value of 2.74  $\mu\text{M}$  while the PBS sample showed the maximum oxygen removal with a value of 23.07  $\mu\text{M}$ . Moreover, the average oxygen removal in all shots is 14.10  $\mu\text{M}$ .

The film results allowed for the estimation of radiation doses at positions behind the sample, revealing a range of dose values for each shot, spanning from 13.63 Gy to 115.91 Gy. Comparing these dose values to the average oxygen removal in the irradiated samples yielded values ranging from 0.30  $\mu\text{M}/\text{Gy}$  to 0.42  $\mu\text{M}/\text{Gy}$ , as presented in figure 5.16 and table 5.8. Among the samples, the PBS sample exhibited the highest average oxygen removal, with a value of 0.42  $\mu\text{M}/\text{Gy}$ . Both fully oxygenated water and lysed cell samples displayed the same level of average oxygen removal, with a value of 0.31  $\mu\text{M}/\text{Gy}$ . The culture medium sample showed the lowest average oxygen removal, with a value of 0.30  $\mu\text{M}/\text{Gy}$ .

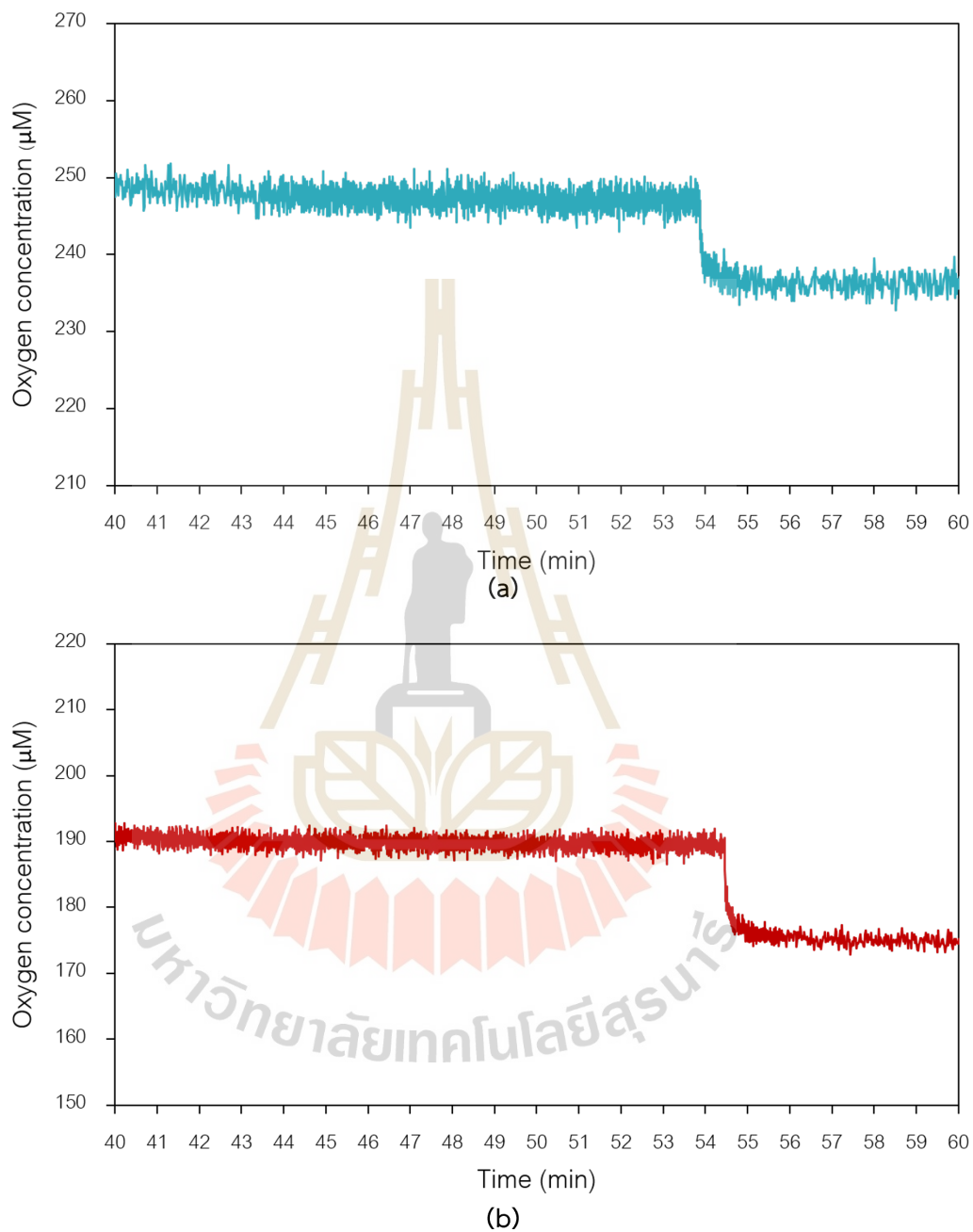


**Figure 5.12** The graph examples of the oxygen removal in irradiated (a) water and (b) PBS from the irradiation by PHELIX laser-accelerated electrons. Graphs showed oxygen levels drop rapidly during the irradiation.

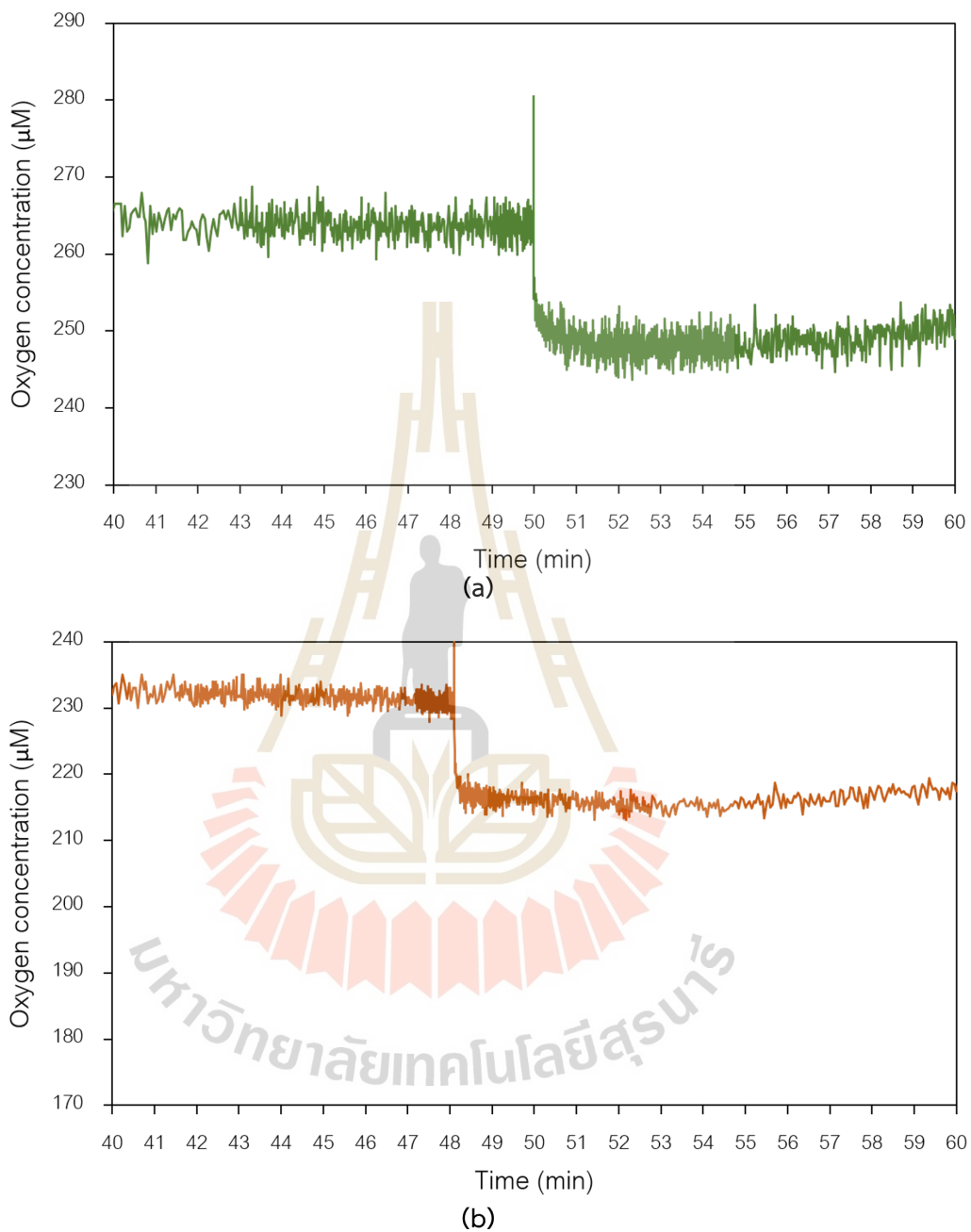


**Figure 5.13** The graph examples of the oxygen removal in irradiated (a) cell culture medium and (b) lysed cells from the irradiation by PHELIX laser-accelerated electrons. Graphs showed oxygen levels drop rapidly during the irradiation.

**Table 5.7** The average oxygen removal of irradiated samples in four different types of samples from PHELIX laser-accelerated electron experiments.

Samples	Number of shots	Average oxygen removal [ $\mu\text{M}$ ]
Water	4	12.15
PBS	4	15.10
Culture medium	5	13.66
Lysed cells	5	15.30
Total shots	18	14.10

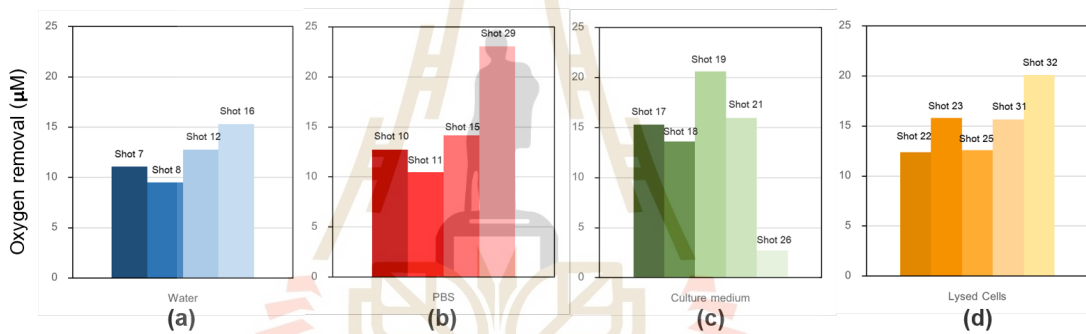


**Figure 5.14** The oxygen removal in irradiated samples after irradiation with laser-accelerated electrons in each shot divided by four different sample groups consisting of (a) water, (b) PBS, (c) cell culture medium and (d) lysed cells.

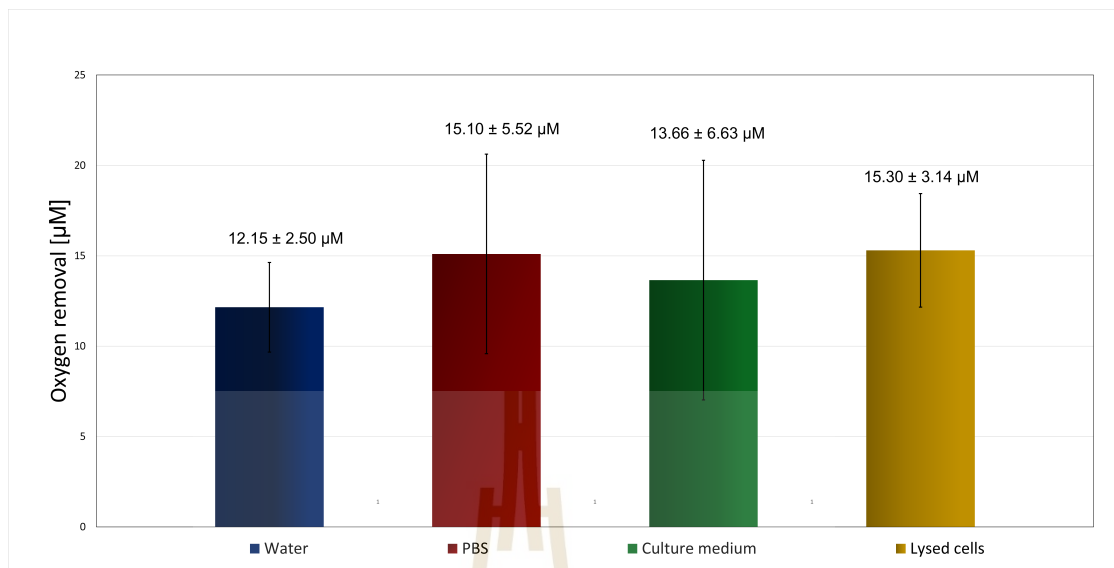


**Figure 5.15** The average oxygen removal in irradiated samples after irradiation with laser-accelerated electrons divided by four different sample groups consisting of water, PBS, cell culture medium and lysed cells.

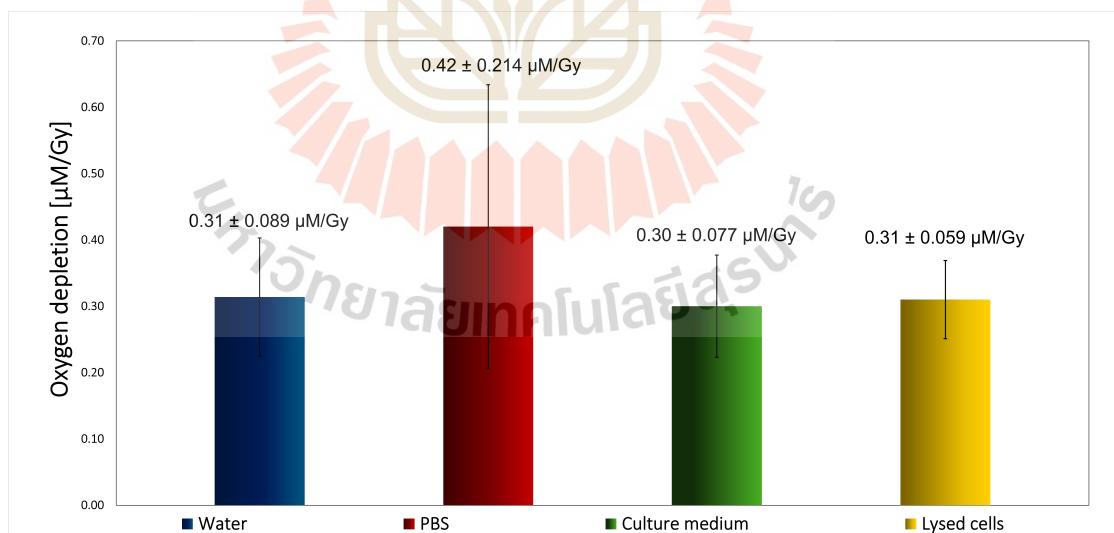
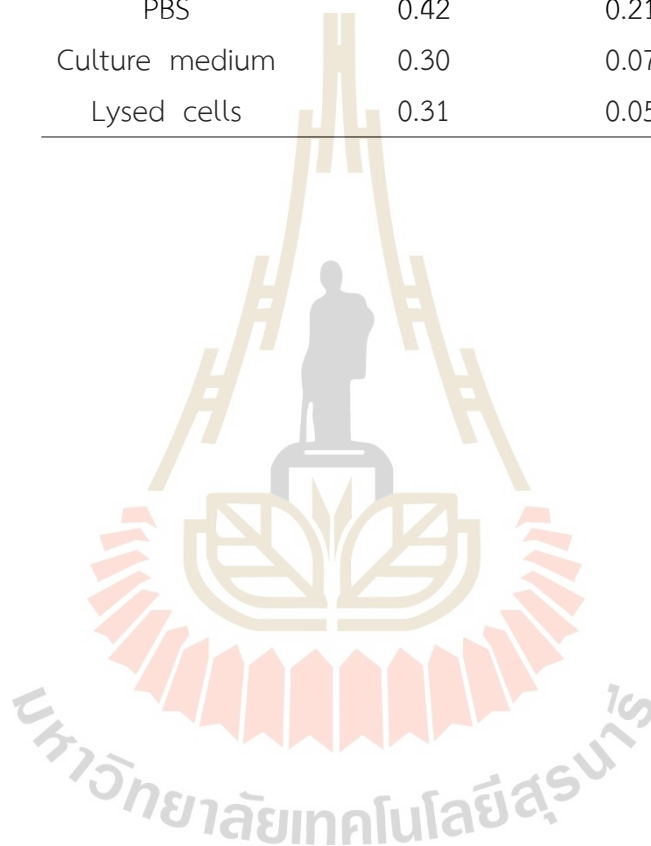


**Figure 5.16** The average oxygen removal of irradiated samples from PHELIX laser-accelerated electron after estimating the radiation dose divided by four different sample groups consisting of water, PBS, cell culture medium and lysed cells.

**Table 5.8** The average oxygen removal of irradiated samples in four different types of samples from PHELIX laser-accelerated electron experiments after estimating the radiation dose.

Samples	Average oxygen removal [ $\mu\text{M}/\text{Gy}$ ]	Standard deviation
Water	0.31	0.089
PBS	0.42	0.214
Culture medium	0.30	0.077
Lysed cells	0.31	0.059



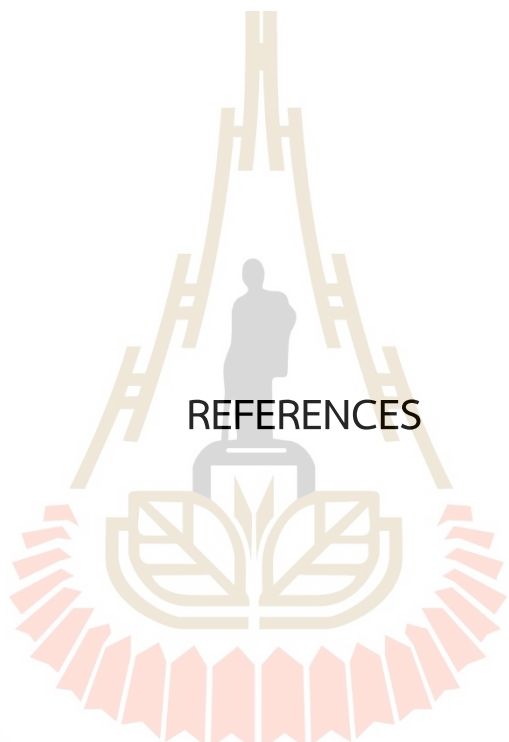
## CHAPTER VI

### CONCLUSION AND DISCUSSION

This study aims to verify oxygen removal during irradiation in different samples using two distinct dose rate ranges: X-ray beams for irradiation with a low dose rate range (CONV) and electron beams for irradiation with an ultrahigh dose rate (FLASH). The samples were divided into two main categories: water (including full oxygenated water and deoxygenated water) and biochemical samples (PBS, culture medium, and lysed cells). Preliminary experiments were conducted to ensure the suitability of the experimental setup. In the experimental study of irradiation with low dose rate ranges and short intervals of irradiation time (5 minutes). The oxygen removal during the irradiation had the highest value in the first irradiation step, which was consistent across all irradiated samples. The maximum value of the average oxygen removal is in the irradiated cell culture medium with a value of 0.42  $\mu\text{M}/\text{Gy}$  and has slightly different quantities in full oxygenated water, deoxygenated water, PBS and lysed cell samples with values of 0.28, 0.26, 0.26 and 0.27  $\mu\text{M}/\text{Gy}$ , respectively. From these experimental results, we confirmed that the oxygen concentration in all samples decreased during the X-ray irradiation. It is in agreement with the previous research, in which the cell culture medium had greater oxygen removal than buffered water (Evans, 1969; Whillans and Rauth, 1980). In addition, our data show that the oxygen removal in the cell culture medium was significantly noticed when compared with full oxygenated water ( $P < 0.05$ ) in the third irradiation step. Calculating the significance between five sample groups was performed using the One-Way ANOVA test in GraphPad Prism Software (version 8.02; GraphPad Software, Inc.). We considered that the highest oxygen depletion in the culture medium was caused by the presence of a wide variety of organic molecules such as fatty acids and amino acids. They have reactions with other radicals during the irradiation such as the reaction with hydroxy radicals ( $\text{OH}^\bullet$ ). From this reaction, the organic molecule is changed to organic radical  $\text{R}^\bullet + \text{H}_2\text{O}$  and then reacts with the oxygen molecule (Boscolo et al., 2021). Moreover, in general, solvated electrons ( $e_{\text{aq}}^-$ ) and hydrogen radicals ( $\text{H}^\bullet$ ) are produced throughout

each step of irradiation. These are two primary species that can interact with oxygen molecules and transform into superoxide ( $O_2^{\bullet-}$ ) and perhydroxyl radicals ( $HO_2^{\bullet-}$ ). These radicals which still remain can react with the new radicals in the next irradiation step competing with the oxygen, resulting in oxygen removal decreasing (Boscolo et al., 2020). Subsequently, the experiment conducted with a longer interval time (1–5 hr) demonstrated that the average oxygen removal was consistent between the first and second irradiation steps. This observation can be attributed to the fact that the radicals generated during the first irradiation step had already formed stable molecules prior to the commencement of the second step. Consequently, there were no radicals to compete with the oxygen molecules to react and create the new radiolytic radical in the second irradiation step.

For the irradiation with laser-accelerated electron or FLASH irradiation, due to the limitations of the irradiation shots, deoxygenated water samples were not used in this experiment in order to increase the experimental repetition and obtain more reliable results. Full oxygenated water, PBS, cell culture medium and lysed cell samples were exposed to the accelerated electron and found to instantly drop their oxygen levels during the irradiation. The dose analysis is still in progress using Monte Carlo simulation. The estimated delivered dose ranged between 30–35 Gy, with an irradiation duration of 20 ps per shot. Based on the available data, the average oxygenation reduction per irradiation step was estimated to be 12.15, 15.10, 13.66 and 15.30  $\mu\text{M}$  in the full oxygenated water, PBS, cell culture medium and lysed cell samples, respectively. Although radiation doses were estimated, the data are not fully conclusive because the uncertainty for the PHELIX experiment is very high. Therefore, it is currently not possible to determine the final trend of oxygen removal with the FLASH dose rate.



REFERENCES

มหาวิทยาลัยเทคโนโลยีสุรนารี

## REFERENCES

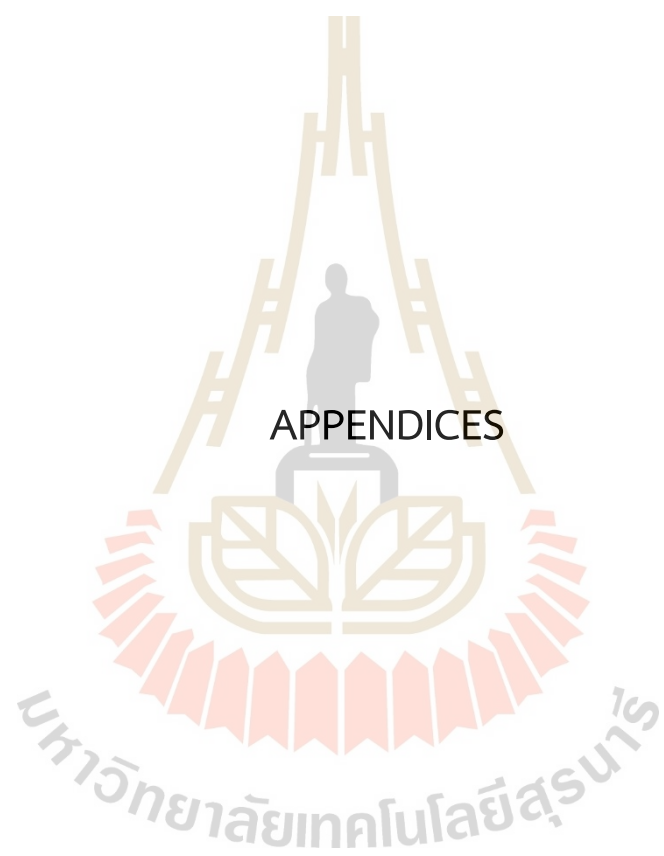
- Adrian, G., Konradsson, E., Lempart, M., Bäck, S., Ceberg, C., and Petersson, K. (2019). The flash effect depends on oxygen concentration. *The British journal of radiology*, *93*, 20190702.
- Alemany Ribes, M., Garcia-Diaz, M., Acedo, P., Agut, M., Nonell, S., Sagristá, M., M, M., Cañete, M., A, V., Stockert, J., and Semino, C. (2013). Why not introducing the third dimension in photodynamic therapy research? *Analytical Bioanalytical Techniques*.
- Allisy, A., Jennings, W. A., Kellerer, A. M., and Müller, J. W. (1993). Report 51. *Journal of the International Commission on Radiation Units and Measurements*, *os26(2)*, NP.
- Ast, C., Schmäzlin, E., Löhmannsröben, H.-G., and Van Dongen, J. T. (2012). Optical oxygen micro- and nanosensors for plant applications. *Sensors*, *12(6)*, 7015–7032.
- Boscolo, D., Krämer, M., Fuss, M. C., Durante, M., and Scifoni, E. (2020). Impact of target oxygenation on the chemical track evolution of ion and electron radiation. *International Journal of Molecular Sciences*, *21(2)*, 424.
- Boscolo, D., Scifoni, E., Durante, M., Krämer, M., and Fuss, M. C. (2021). May oxygen depletion explain the flash effect? a chemical track structure analysis. *Radiotherapy and Oncology*, *162*, 68–75.
- Bourhis, J., Sozzi, W. J., Jorge, P. G., Gaide, O., Bailat, C., Duclos, F., ..., and Vozenin, M. C. (2019). Treatment of a first patient with flash-radiotherapy. *Radiotherapy and oncology : journal of the European Society for Therapeutic Radiology and Oncology*, *139*, 18–22.
- Bushberg, J. T., Seibert, A. J., Leidholdt, E. M., and Boone, J. M. (2005). *Radiation oncology physics: A handbook for teachers and students*. International Atomic Energy Agency (IAEA).

- Bushberg, J. T., Seibert, A. J., Leidholdt, E. M., and Boone, J. M. (2012). *The essential physics of medical imaging; 4th ed.* Lippincott Williams Wilkins, Philadelphia, PA.
- Cancer Research UK (2020). Cancer cells. [Online]. Retrieved from <https://www.cancerresearchuk.org/about-cancer/what-is-cancer/how-cancer-starts/cancer-cells>.
- Dewey, D. L. Boag, J. W. (1959). Modification of the oxygen effect when bacteria are given large pulses of radiation. *Nature*, 183, 1450–1451.
- Epp, E. R., Weiss, H., Djordjevic, B., and Santomasso, A. (1972). The radiosensitivity of cultured mammalian cells exposed to single high intensity pulses of electrons in various concentrations of oxygen. *Radiation Research*, 52(2), 324–332.
- Evans, N. T. S. (1969). Removal of dissolved oxygen from aqueous media by ionizing radiations. *Radiation Effects*, 1(1), 19–22.
- Favaudon, V., Caplier, L., Monceau, V., Pouzoulet, F., Sayarath, M., Fouillade, C., ..., and Vozenin, M. C. (2014). Ultrahigh dose-rate flash irradiation increases the differential response between normal and tumor tissue in mice. *Science translational medicine*, 6(245), 245ra93.
- Field, S. B. and Bewley, D. K. (1974). Effects of dose-rate on the radiation response of rat skin. *International Journal of Radiation Biology and Related Studies in Physics, Chemistry and Medicine*, 26(3), 259–267.
- Gray, L. H., Conger, A. D., Ebert, M., Hornsey, S., and Scott, O. C. (1953). The concentration of oxygen dissolved in tissues at the time of irradiation as a factor in radiotherapy. *The British journal of radiology*, 26(312), 638–648.
- GSI Helmholtz Centre for Heavy-Ion Research GmbH (2021). Perspectives for future tumor therapy: New flash method for ultrafast, high-dose heavy ion irradiation tested for the first time. [Online]. Retrieved from <https://www.eurekalert.org/pub,leases/2021-06/ghfs-pff062121.php>.

- GSI Helmholtz Centre for Heavy-Ion Research GmbH (n.d.). Phelix laser facility. [Online]. Retrieved from [https://www.gsi.de/en/work/research/appamml/plasma\\_physics/phelix/phelix](https://www.gsi.de/en/work/research/appamml/plasma_physics/phelix/phelix).
- Hornsey, S. and Bewley, D. (1971). Hypoxia in mouse intestine induced by electron irradiation at high dose-rates. *International Journal of Radiation Biology and Related Studies in Physics, Chemistry and Medicine*, 19(5), 479–483.
- Howard-Flanders, P. and Moore, D. (1958). The time interval after pulsed irradiation within which injury to bacteria can be modified by dissolved oxygen: I. a search for an effect of oxygen 0.02 second after pulsed irradiation. *Radiation Research*, 9(4), 422–437.
- Hughes, J. R. and Parsons, J. L. (2020). Flash radiotherapy: Current knowledge and future insights using proton-beam therapy. *International Journal of Molecular Sciences*, 21(18).
- INTERNATIONAL ATOMIC ENERGY AGENCY (2001). *Absorbed Dose Determination in External Beam Radiotherapy*. IAEA.
- Lareau, S. C. and Fahy, B. (2020). Oxygen therapy. [Online]. Retrieved from <https://www.thoracic.org/patients/patient-resources/resources/oxygen-therapy.pdf>.
- Le Caër, S. (2011). Water radiolysis: Influence of oxide surfaces on h<sub>2</sub> production under ionizing radiation. *Water*, 3(1), 235–253.
- McKeown, S. R. (2014). Defining normoxia, physoxia and hypoxia in tumours-implications for treatment response. *The British journal of radiology*, 87(1035), 20130676.
- Medina, L.-A., Herrera-Penilla, B.-I., Castro-Morales, M.-A., García-López, P., Jurado, R., Pérez-Cárdenas, E., Chanona-Vilchis, J., and Brandan, M.-E. (2008). Use of an orthovoltage x-ray treatment unit as a radiation research system in a small-animal cancer model. *Journal of Experimental Clinical Cancer Research*, 27, 57.
- Muz, B., de la Puente, P., Azab, F., and Azab, A. K. (2015). The role of hypoxia in cancer progression, angiogenesis, metastasis, and resistance to therapy. *Hypoxia (Auckland, N.Z.)*, 3, 83–92.

- Omyan, G., Musa, A. E., Shabeeb, D., Akbardoost, N., and Gholami, S. (2020). Efficacy and toxicity of flash radiotherapy: A systematic review. *Journal of cancer research and therapeutics*, 16(6), 1203–1209.
- Pastina, B. and LaVerne, J. A. (2001). Effect of molecular hydrogen on hydrogen peroxide in water radiolysis. *The Journal of Physical Chemistry A*, 103(40), 9316–9322.
- Petersson K, Adrian G, B. K. M. S. (2020). A quantitative analysis of the role of oxygen tension in flash radiation therapy. *International Journal of Radiation Oncology, Biology, Physics*, 107(3), 539–547.
- Pittman, R. N. (2011). Regulation of tissue oxygenation. In *Colloquium series on integrated systems physiology: from molecule to function*, 3(3), 1–100.
- PreSens Precision Sensing GmbH (2015). Compact trace oxygen meter with analog output. [Online]. Retrieved from <https://www.presens.de/products/detail/oxy-1-sma-trace-rs232-ao>.
- PreSens Precision Sensing GmbH (n.d.). The stern-volmer relationship [Online]. Retrieved from <https://www.presens.de/knowledge/basics/detail/the-stern-volmer-relationship-900>.
- Ramachandran, S., lent, J., Göttgens, E.-L., Krieg, A., and Hammond, E. (2015). Epigenetic therapy for solid tumors: Highlighting the impact of tumor hypoxia. *Genes*, 6, 935–956.
- reports series, T. (2008). *Relative Biological Effectiveness in Ion Beam Therapy*. INTERNATIONAL ATOMIC ENERGY AGENCY, Vienna.
- Schardt, D., Elsässer, T., and Schulz-Ertner, D. (2010). Heavy-ion tumor therapy: Physical and radiobiological benefits. *Reviews of Modern Physics*, 82(1), 383–425.
- Schüller, A., Heinrich, S., Fouillade, C., Subiel, A., De Marzi, L., Romano, F., ..., and MVozenin, M.-C. (2020). The european joint research project uhdpulse – metrology for advanced radiotherapy using particle beams with ultra-high pulse dose rates. *Physica Medical*, 80, 134–150.

- Staff, H. (2020). Hemoglobin. [Online]. Retrieved from <https://www.cigna.com/individuals-families/health-wellness/hw/hemoglobin-tp10337>.
- Vozenin, M. C., De Fornel, P., Petersson, K., Favaudon, V., Jaccard, M., Germond, J. F., Petit, B., Burki, M., Ferrand, G., Patin, D., Bouchaab, H., Ozsahin, M., Bochud, F., Bailat, C., Devauchelle, P., and Bourhis, J. (2019). The advantage of flash radiotherapy confirmed in mini-pig and cat-cancer patients. *Clinical cancer research*, 25(1), 35–42.
- Weiss, H., Epp, E. R., Heslin, J. M., Ling, C. C., and Santomasso, A. (1974). Oxygen depletion in cells irradiated at ultra-high dose-rates and at conventional dose-rates. *International Journal of Radiation Biology and Related Studies in Physics, Chemistry and Medicine*, 26(1), 17–29.
- Whillans, D. W. and Rauth, A. M. (1980). An experimental and analytical study of oxygen depletion in stirred cell suspensions. *Radiation Research*, 84(1), 97–114.
- Zähler, Ş. J. (2020). *Development of FAIR-relevant X-ray diagnostics based on the interaction of lasers and particle beams with matter*. doctoralthesis, Universitätsbibliothek Johann Christian Senckenberg.
- Zakaria, A. M., Colangelo, N. W., Meesungnoen, J., Azzam, E. I., Plourde, M., and Jay-Gerin, J. P. (2020). Ultra-high dose-rate, pulsed (flash) radiotherapy with carbon ions: Generation of early, transient, highly oxygenated conditions in the tumor environment. *Radiation research*, 194(6), 587–593.



APPENDICES

## APPENDIX A

### CALIBRATION FOR EXPERIMENT

#### A.1 Calibration for X-ray irradiation experiment

These calibrations were used in the X-ray irradiation experiments. Cables with lengths of 1.5 and 2.5 m were connected together with a screw to measure the oxygen level. Calibrations of large (P1 and P5) and small containers were showed in tables A.1 and A.2.

**Table A.1** Cal 0 and Cal 100 calibration of P1 and P5 containers.

Calibration for large container		Container	
		P1	P5
Cal 0	Phase [°]	57.06	58.75
	Temperature [°C]	21.10	21.40
	Pressure [hPa]	1011.12	1011.69
Cal 100	Phase [°]	25.57	26.28
	Temperature [°C]	23.40	21.70
	Pressure [hPa]	986.0	1011.92

**Table A.2** Cal 0 and Cal 100 calibration for a small container.

Calibration for small container container		
Cal 0	Phase [°]	54.93
	Temperature [°C]	21.0
	Pressure [hPa]	1011.53
Cal 100	Phase [°]	22.27
	Temperature [°C]	23.20
	Pressure [hPa]	986.0

## A.2 Calibration for laser-accelerated electrons irradiation experiment

These calibrations were operated under the vacuum system in order to adapt the system in the actual experiment. Cables were connected together with a feedthrough which connects the vacuum chamber system to the oxygen level measurement installed outside the chamber.

**Table A.3** Cal 0 and Cal 100 calibration of a small container in the vacuum condition.

Calibration for laser-accelerated electrons experiment		
	Phase [ $^{\circ}$ ]	54.40
Cal 0	Temperature [ $^{\circ}$ C]	22.44
	Pressure [hPa]	1016
	Phase [ $^{\circ}$ ]	23.45
Cal 100	Temperature [ $^{\circ}$ C]	22.25
	Pressure [hPa]	1016

## APPENDIX B

### CONFERENCES AND PRESENTATIONS

#### B.1 List of oral presentation

Pharewa Karoon, Chinorat Kobdaj, Chutima Talabnin, and Martina Christina Fuss. (June 2022). Experimental study of radiolytic oxygen removal in irradiated water. **The 17<sup>th</sup> Siam Physics Congress 2022**, Nakhon Ratchasima, Thailand.

Pharewa Karoon, Chinorat Kobdaj, Chutima Talabnin, and Martina Christina Fuss. (April 2023). Experimental Study of Radiolytic Oxygen Depletion from X-Ray Irradiation in Water and Liquid Samples. **The 8<sup>th</sup> RSU International Research Conference on Sciences and Technology 2023**, Pathum Thani, Thailand.



Figure B.1 The certificate of participation in the The 17<sup>th</sup> Siam Physics Congress 2022



Figure B.2 The certificate of participation in the 8<sup>th</sup> RSU International Research Conference on Sciences and Technology 2023



## Experimental Study of Radiolytic Oxygen Depletion from X-ray Irradiation in Water and Liquid Samples

Pharewa Karoon<sup>1</sup>, Chinorat Kobdaj<sup>1</sup>, Chutima Talabnin<sup>2</sup>, Martina Christina Fuss<sup>3</sup>

<sup>1</sup>School of Physics, Institute of Science, Suranaree University of Technology, Nakhon Ratchasima, Thailand

<sup>2</sup>School of chemistry, Institute of Science, Suranaree University of Technology, Nakhon Ratchasima, Thailand

<sup>3</sup>Biophysics Department, GSI Helmholtzzentrum für Schwerionenforschung, Darmstadt, Germany

\*Corresponding author, E-mail: pharephkr@gmail.com

### Abstract

The mechanism underlying the reduction of toxicity in normal tissue caused by ultra-high dose rate irradiation (FLASH) is being investigated but still unknown. Oxygen depletion or the interaction of radiation-induced radicals with dissolved oxygen during irradiation may explain the FLASH effect. In this study, various liquid samples, including full oxygenated water, deoxygenated water, phosphate-buffered saline (PBS) and Ham's F12 cell culture medium were irradiated with conventional dose rates to investigate experimental oxygen depletion in samples. The radiation-induced radical production and reactions were examined as a reference, before studying the oxygen depletion with FLASH irradiation. Samples were exposed to 50 Gy of X-ray radiation at a dose rate of 4.5–10.4 Gy/min. X-ray source dosimetry was performed using a Semiflex ionization chamber. A chemical optical sensor was used to measure the amount of oxygen, and the results were recorded online. The oxygen depletion was highest in the first irradiation step. The result showed that the depletion of oxygen in Ham's F12 cell culture medium was highest with the value of 0.42  $\mu\text{M}/\text{Gy}$ . Deoxygenated water and phosphate-buffered saline (PBS) had the lowest oxygen depletion with the value of 0.26  $\mu\text{M}/\text{Gy}$ . For the irradiation in the second step, the results showed a similar trend of oxygen depletion that was lower than the first step and lowest depletion occurred in the third step of irradiation. We conclude that radical production and reactions, which compete with oxygen depletion, cause the declining behavior of oxygen depletion. Additionally, solutions containing organic compounds showed a greater depletion of oxygen.

**Keywords:** X-ray irradiation, FLASH irradiation, FLASH effect, Oxygen depletion

### 1. Introduction

One essential part of the cancer treatments available today is radiotherapy. Although it is well established for clinical treatment, irradiation at conventional dose rates (CONV) ( $\sim 2$  Gy/min) takes time to deliver the treatment. Moreover, the irradiation process damages not only tumor cells but also normal tissues.

In fact, the irradiation experiment with ultrahigh dose rates has been reported since the 1950s (Dewey & Boag, 1959; Town, 1967; Hornsey & Bewley, 1971), and the term of "FLASH" irradiation (in excess of 40 Gy/s) was applied in 2014 and has gained much focus over the last few years. The *in vivo* experiment using FLASH irradiation was performed in a mice tissue. The result showed radio-protection in the normal tissues while preserving cytotoxicity in tumor tissues. This normal tissue sparing effect is referred to as the FLASH effect (Favaudon et al., 2014). Currently, there are different FLASH sources consisting of photons, electrons protons and carbon ions (Montay-Gruel et al., 2018; Liljedahl et al., 2022; Sørensen et al., 2022; Tinganelli et al., 2022). Although FLASH irradiation has been demonstrated, both *in vivo* and *in vitro* (Vozenin et al., 2019; Adrian et al., 2020; Hageman, Che, Dachele, Slotman, & Sminia, 2022), but the mechanism behind the FLASH effect is still unclear. Recently, the first human trial showed that FLASH therapy was effective in treating cancer, but its efficacy was comparable to conventional radiation therapy (Bourhis et al., 2019; Gaide et al., 2022). Oxygen depletion is thought to be the FLASH mechanism (Adrian et al., 2020; Pratz & Kapp, 2019).

Oxygen is a powerful radiosensitizer that generates a free radical molecule that has efficiency for DNA damage (Liu et al., 2015). Several studies demonstrated that the cells in hypoxic conditions, or with

[18]



hypoxic areas, are up to three times more radioresistant than normal cells at the well-oxygenated level (Grimes & Partridge, 2015). During irradiation, ionizing radiation induced water radiolysis cause the dissociation of water molecules, which leads to the loss of dissolved oxygen (Le Caër, 2011; Boscolo, Krämer, Fuss, Durante, & Scifoni, 2020) and generates a wide range of chemical species in a short period of time. Hydrogen radicals and solvated electrons are among the major apparent products of irradiation. These radiolytic species can interact with molecular oxygen dissolved in water, then produce the perhydroxyl ( $\text{HO}_2^{\cdot}$ ) radical and superoxide ( $\text{O}_2^{\cdot-}$ ) resulting in a decrease in oxygen concentration. Early findings in oxygen measurements in bacteria and mammalian cells showed that oxygen depletion can lead to significant at very high dose rate sparing by having the cell survival curves behave as in a hypoxic condition during irradiation (Epp, Weiss, Djordjevic, & Santomaso, 1972; Weiss, Epp, Heslin, Ling, & Santomaso, 1974). Moreover, investigations of oxygen depletion have recently been published as part of experiments and simulations (Jansen et al., 2021; Boscolo, Scifoni, Durante, Krämer, & Fuss, 2021).

In this study, we investigated the oxygen depletion in irradiated water and liquid samples consisting of full oxygenated water, deoxygenated water, phosphate-buffered saline (PBS) and Ham's F12 cell culture medium with CONV dose rate range. X-ray beam was used as the radiation source since it is the typical beam that is usually used for the CONV radiotherapy.

## 2. Objectives

- 1) To investigate oxygen depletion in irradiated samples such as full oxygenated water, deoxygenated water, phosphate-buffered saline (PBS) and the cell culture medium.
- 2) To compare oxygen depletion between the different samples.
- 3) To examine the radical production and reactions that occur from the x-ray irradiated samples and keep the data as a reference before doing the experiment on FLASH irradiation.

## 3. Materials and Methods

### 3.1 Instruments for oxygen measurement

For the experimental section of this study, almost all the equipment involved in this oxygen depletion measurement was from PreSens Precision Sensing GmbH (Germany). There were two types of containers used in this experiment. The first container was the main container for X-ray irradiation only. It was designed for non-vacuum conditions which could be reused and cleaned (see Figure 1(a)). The second container was the cylindrical container as shown in Figure 1(b). It was designed for both X-ray and FLASH irradiation. Each container, the sensor spot with a diameter of 5 mm (SP-Pst3-SA23-D5-OIW-US) was glued on the inner wall. This sensor spot contains luminophores for detecting the oxygen molecules dissolved in the samples (Ast, Schmälzlin, Löhmannsröben, & van Dongen, 2012). During the measurement, the oxygen concentration was monitored and collected by a compact oxygen meter system (OXY-1 SMA-trace-RS232-AO) and the PreSens.EOM STS software. The LED in this oxygen meter excites the sensor spot at a 505 nm wavelength. After that, the oxygen meter processor continued to work based on the phase signal. The changes in oxygen concentration inside the samples were measured with a time resolution of 1 s.

### 3.2 Container setups and samples preparation

Two types of container were used in this experiment, the main container and the cylindrical container. The main container had the benefit of being reusable. The cylindrical container was airtight and used in vacuum conditions. The main container consisted of five parts: a spot sensor, a holder, an inset, a rubber stopper and a plastic container. The spot sensor was located at the center between the plastic container and the inset. The optical fiber was connected to the plastic container via a holder piece, which was placed in the same location as the spot sensor. The inset was an area for filling samples. One side of the inset was opened to allow the sensor spot to contact the sample. Before inserting the inset inside the plastic container, we coated the exterior of the inset with a moisture-curing silicone rubber (ELASTOSIL® E43 TRANSPARENT). The rubber stopper was then used to seal the inset compartment, keeping it airtight and

[19]

preventing the diffusion of oxygen. The inset can hold a sample with a volume of approximately  $1 \text{ cm}^3$ . The total height of the main container, including the lid is 5.4 cm.

The cylindrical containers (see Figure 1(b)) were prepared for both X-rays and FLASH experiments. It consists of three cylindrical components. The top part has been tapped with a threading for mounting a screw to maintain the proper position of the container. The middle part is a one-open-end cylinder with a 5 mm inner diameter and a 5 mm depth. At the open end, it is covered with a thin piece of transparent plastic with a spot sensor placed underneath. Another side of the cylinder has a tiny hole for filling the container with the sample using a syringe. The bottom part is an optical fiber holder that allows the optical fiber to make a contact with the sensor spot.

An inset piece of the main container and three pieces of the cylindrical container were made in the GSI Helmholtz Center for Heavy Ion Research (GSI) workshop using polyetheretherketone (PEEK) material. It is resistant to radiation and chemicals. When exposed to radiation, it does not leach chemicals or oxygen.

Samples were prepared differently depending on their properties. Full oxygenated water, phosphate-buffered saline (PBS) and cell culture medium (Ham's F12) do not need any special preparation. They can be filled directly into containers. However, for the deoxygenated water, nitrogen gas was added into the full oxygenated water for 10–15 minutes to decrease the oxygen concentration from 250–320  $\mu\text{M}$  to 189–235  $\mu\text{M}$ .

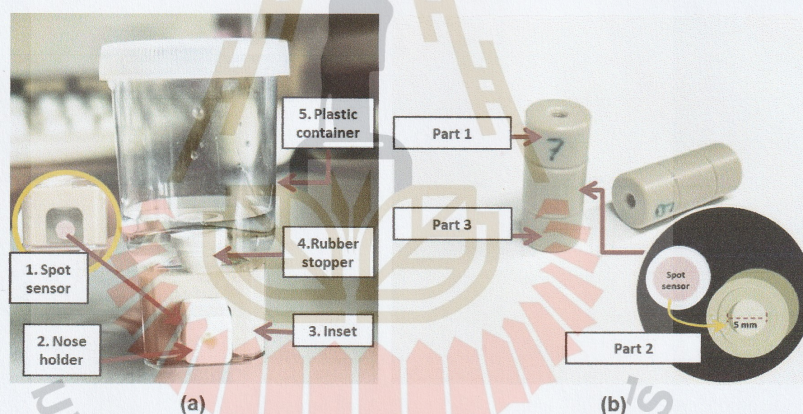


**Figure 1** Apparatus of the study: (a) the main container for X-ray irradiation used to contain the water and PBS samples; (b) The cylindrical containers with an inner diameter of 5 mm and a depth of 5 mm used for FLASH experiments in vacuum conditions.

### 3.3 X-ray beam and dosimetry

To investigate the oxygen depletion at the conventional dose rate, the samples with the sensor spots were irradiated using a 250 kV X-ray beam at the GSI Helmholtz Centre for Heavy Ion Research, Germany at a dose rate of 4.5–4.8 Gy/min for the large container and 10.0–10.4 Gy/min for the cylindrical container. The dosimetry for the X-ray irradiation was carried out using a Semiflex ionization chamber (IC, type number TM31013, PTW, Germany).

### 3.4 Experimental setup

For the irradiation, both containers were fully filled with samples without air bubbles and completely closed. Containers were placed under the X-ray target and beside the Semiflex chamber. On the outside of the container wall, the optical fiber with a total length of 4 meters was placed to connect between the sensor

[20]

spot and the oxygen meter. The oxygen meter was then linked to the computer for data collection. Figure 2 shows the experimental setup for X-ray radiation. A calibration was done for the oxygen meter prior to use in the specific set-up (with respective container, cable length and connectors).

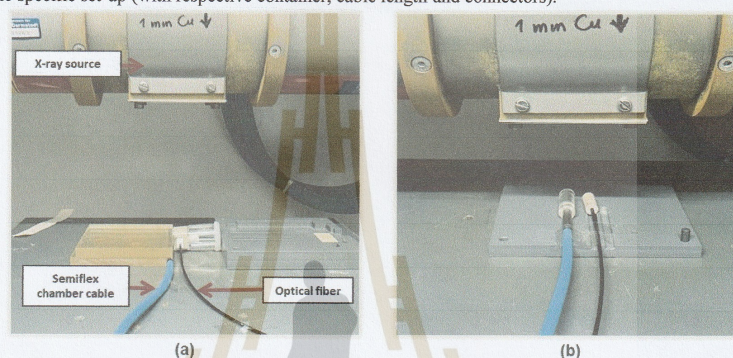


**Figure 2** Set up of GSI X-ray machine for irradiation with a 250 kV photon. The dose dosimetry was carried out by the Semiflex chamber (IC, type number TM31013, PTW, Germany). (a) The dosimeter was placed under a Polymethyl Methacrylate (PMMA) slab beside the main container. (b) The dosimeter was enclosed with the dosimeter's build-up cap and placed beside the cylindrical container

### 3.5 Statistical analysis

Values of oxygen depletion are presented as the average  $\pm$  standard deviation (SD) of the sixteen, seven, seven and three replicated experiments in full oxygenated water, deoxygenated water, PBS and cell culture medium, respectively. Statistical analysis was performed using Microsoft Excel (version: Microsoft 365 Apps for enterprise) and GraphPad Prism Software (version 8.02; GraphPad Software, Inc.). The One-Way ANOVA test was used to calculate the significance between four sample groups. P-values lower than 0.05 were regarded to indicate a statistically significant difference.

### 4. Results and Discussion

The average oxygen concentrations in the samples before the irradiation in full oxygenated water, deoxygenated water, PBS, and cell culture medium were 283.87, 207.42, 290.46, and 224.22  $\mu\text{M}$ , respectively. All samples were irradiated into three steps with a dose of 50 Gy per step. The oxygen concentration was measured and plotted during three consecutive irradiations as shown in Figure 3.

In Figure 4 and Table 1, we showed the relation between the oxygen depletion against the cumulative dose. It was found that the amount of oxygen depletion was highest at the first irradiation and then decreased in the steps afterward. In the case of the full oxygenated water, the average oxygen depletion per dose in the first three steps were 0.28, 0.25 and 0.23  $\mu\text{M}/\text{Gy}$ . For the deoxygenated water, the average oxygen depletion per dose was 0.26, 0.22 and 0.18  $\mu\text{M}/\text{Gy}$ , respectively. The average oxygen depletion per dose in PBS was 0.26  $\mu\text{M}/\text{Gy}$  in the first step and then decreases to close to the full oxygenated water with values of 0.26 and 0.23  $\mu\text{M}/\text{Gy}$  in the second and third steps of irradiation. The cell culture medium showed the average oxygen depletion per dose were 0.42, 0.38 and 0.37  $\mu\text{M}/\text{Gy}$  in the first, second and third steps of irradiation, respectively. According to our findings, the oxygen depletion was significantly observed in culture medium when compared with full oxygenated water ( $P < 0.05$ ). It is consistent with the previous study in which the oxygen depletion in the cell medium was greater than that in buffered water (Evans, 1969; Whillans & Rauth, 1980). Apparently, the oxygen depletion in the cell culture medium was the highest in all three steps of

[21]

irradiation. We considered that the largest oxygen depletion in cell culture medium was due to the presence of several organic molecules such as fatty acids and amino acids. The reaction between the organic molecules and other radicals is possible, such as the reaction with hydroxyl radicals ( $\text{OH}^\bullet$ ).  $\text{OH}^\bullet$  changes the organic molecule to the organic radical  $\text{R}^\bullet + \text{H}_2\text{O}$  that is capable of reacting with oxygen (Boscolo, Scifoni, Durante, Krämer, & Fuss, 2021).

In general, each step of irradiation, solvated electrons ( $e_{\text{aq}}^-$ ) and hydrogen radicals ( $\text{H}^\bullet$ ) are created. These are two main species that can interact with oxygen molecules and transform into the superoxide ( $\text{O}_2^{\bullet-}$ ) and perhydroxyl radicals ( $\text{HO}_2^\bullet$ ) (Boscolo et al., 2020). This mechanism results in oxygen depletion in the irradiated samples. For the second irradiation step, there are possibilities that the newly created solvated electrons ( $e_{\text{aq}}^-$ ) and hydrogen radicals ( $\text{H}^\bullet$ ) can interact with not only oxygen molecules but also the previously formed superoxide ( $\text{O}_2^{\bullet-}$ ) and perhydroxyl radicals ( $\text{HO}_2^\bullet$ ). Therefore, the amount of oxygen molecules depleted in the second irradiation step is lower than it was in the first. The same is true for the third irradiation step. It is clearly seen that our experiments have confirmed the above assumption.

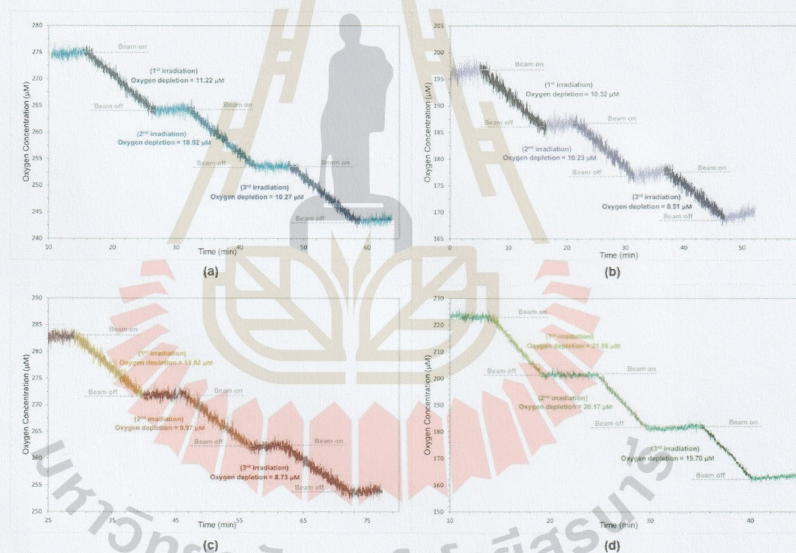


**Figure 3** Example curves of the oxygen concentration during three irradiations: (a) full oxygenated water, (b) deoxygenated water, (c) PBS, and (D) cell culture medium. Samples were irradiated for three steps with 50 Gy/step

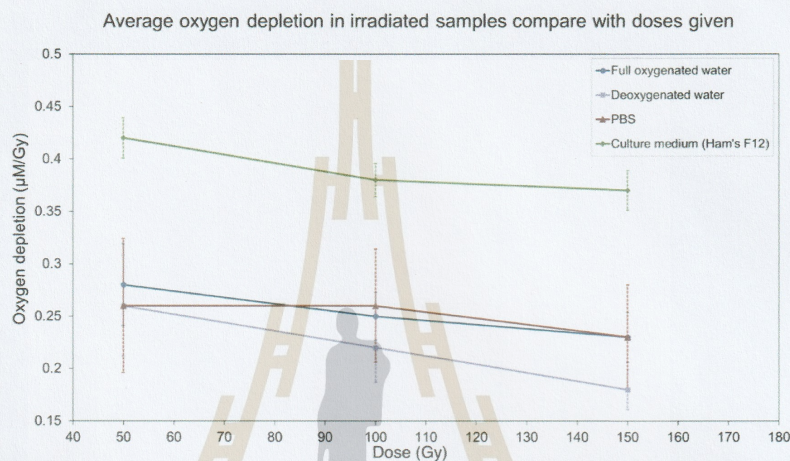


**Figure 4** Comparison of the average oxygen depletion against the cumulative doses. In this graph, each line has three points. The first point represents the average oxygen depletion when the sample was irradiated with a dose of 50 Gy. The second and third points represent the average oxygen depletion during the second and third steps of irradiation (50 Gy)

**Table 1** Average oxygen depletion in irradiated samples compared to the cumulative doses

Cumulative doses (Gy)	Oxygen depletion (µM/Gy)			
	Full oxygenated water	Deoxygenated water	PBS	Ham's F12
50	0.28 ± 0.039	0.26 ± 0.048	0.26 ± 0.064	0.42 ± 0.019
100	0.25 ± 0.023	0.22 ± 0.033	0.26 ± 0.054	0.38 ± 0.016
150	0.23 ± 0.024	0.18 ± 0.019	0.23 ± 0.050	0.37 ± 0.019

## 5. Conclusion

The investigation of oxygen depletion during conventional (CONV) irradiation utilizing a conventional dose rate had been performed. Different samples have been irradiated with an X-ray beam at a dose of 50 Gy/step. The experimental results confirmed that the oxygen concentration in all samples decreased during the X-ray irradiation. The data on oxygen depletion was kept as a reference for comparison with the results of the experiment with laser-accelerated electron irradiation in the future.

## 6. Acknowledgements

This work was supported by (i) Suranaree University of Technology (SUT), (ii) Thailand Science Research and Innovation (TSRI) under Grant number IRN62W0006, (iii) National Science Research and Innovation Fund (NSRF) (NRIIS number 160353 and 160355), (iv) Center of Excellence in High Energy Physics and Astrophysics (CoE) and (v) Research center for theoretical Physics (RU). P Karoon is also funded by DPST (Development and Promotion of Science and Technology Talents Project, Thai government scholarship). This work was carried out in collaboration with GSI/FAIR under GET INVolved program. The authors also thank Dr. Dea Aulia Kartini for her help during the paper writing.

[23]



## 7. References

- Adrian, G., Konradsson, E., Lempart, M., Bäck, S., Ceberg, C., & Petersson, K. (2020). The FLASH effect depends on oxygen concentration. *The British Journal of Radiology*, 93(1106), 20190702. <https://doi.org/10.1259/bjr.20190702>
- Ast, C., Schmäzlin, E., Löhmansröben, H. G., & van Dongen, J. T. (2012). Optical oxygen micro- and nanosensors for plant applications. *Sensors (Basel, Switzerland)*, 12(6), 7015–7032. <https://doi.org/10.3390/s120607015>
- Boscolo, D., Krämer, M., Fuss, M. C., Durante, M., & Scifoni, E. (2020). Impact of Target Oxygenation on the Chemical Track Evolution of Ion and Electron Radiation. *International Journal of Molecular Sciences*, 21(2), 424. <https://doi.org/10.3390/ijms21020424>
- Boscolo, D., Scifoni, E., Durante, M., Krämer, M., & Fuss, M. C. (2021). May oxygen depletion explain the FLASH effect? A chemical track structure analysis. *Radiotherapy and Oncology*, 162, 68–75. <https://doi.org/10.1016/j.radonc.2021.06.031>
- Bourhis, J., Sozzi, W. J., Jorge, P. G., Gaide, O., Bailat, C., Duclos, F., ... & Vozenin, M. C. (2019). Treatment of a first patient with FLASH-radiotherapy. *Radiotherapy and Oncology*, 139, 18–22. <https://doi.org/10.1016/j.radonc.2019.06.019>
- Dewey, D. L., & Boag, J. W. (1959). Modification of the Oxygen Effect when Bacteria are given Large Pulses of Radiation. *Nature*, 183(4673), 1450–1451. <https://doi.org/10.1038/1831450a0>
- Epp, E. R., Weiss, H., Djordjevic, B., & Santomaso, A. (1972). The Radiosensitivity of Cultured Mammalian Cells Exposed to Single High Intensity Pulses of Electrons in Various Concentrations of Oxygen. *Radiation Research*, 52(2), 324–332. <https://doi.org/10.2307/3573572>
- Evans, N. T. S. (1969). Removal of dissolved oxygen from aqueous media by ionizing radiations. *Radiation Effects*, 1(1), 19–22. doi: 10.1080/00337576908234454
- Favaudon, V., Caplier, L., Monceau, V., Pouzoulet, F., Sayarath, M., Fouillade, C., ... & Vozenin, M. C. (2014). Ultrahigh dose-rate FLASH irradiation increases the differential response between normal and tumor tissue in mice. *Science translational medicine*, 6(245), 245ra93. <https://doi.org/10.1126/scitranslmed.3008973>
- Gaide, O., Herrera, F., Sozzi, W. J., Jorge, P. G., Kinj, R., Bailat, C., ... & Bourhis, J. (2022). Comparison of ultra-high versus conventional dose rate radiotherapy in a patient with cutaneous lymphoma. *Radiotherapy and Oncology*, 174, 87–91. <https://doi.org/10.1016/j.radonc.2021.12.045>
- Grimes, D. R., & Partridge, M. (2015). A mechanistic investigation of the oxygen fixation hypothesis and oxygen enhancement ratio. *Biomedical physics & engineering express*, 1(4), 045209. <https://doi.org/10.1088/2057-1976/1/4/045209>
- Hageman, E., Che, P. P., Dachele, M., Slotman, B. J., & Sminia, P. (2022). Radiobiological Aspects of FLASH Radiotherapy. *Biomolecules*, 12(10), 1376. <https://doi.org/10.3390/biom12101376>
- Hornsey, S., & Bewley, D. K. (1971). Hypoxia in Mouse Intestine Induced by Electron Irradiation at High Dose-rates. *International Journal of Radiation Biology and Related Studies in Physics, Chemistry and Medicine*, 19(5), 479–483. <https://doi.org/10.1080/09553007114550611>
- Jansen, J., Knoll, J., Beyreuther, E., Pawelke, J., Skuza, R., Hanley, R., ... & Seco, J. (2021). Does FLASH deplete oxygen? Experimental evaluation for photons, protons, and carbon ions. *Medical physics*, 48(7), 3982–3990. <https://doi.org/10.1002/mp.14917>
- Le Caër, S. (2011). Water Radiolysis: Influence of Oxide Surfaces on H<sub>2</sub> Production under Ionizing Radiation. *Water*, 3(1), 235–253. <https://doi.org/10.3390/w3010235>
- Liljedahl, E., Konradsson, E., Gustafsson, E., Jonsson, K. F., Olofsson, J. K., Ceberg, C., & Redebrandt, H. N. (2022). Long-term anti-tumor effects following both conventional radiotherapy and FLASH in fully immunocompetent animals with glioblastoma. *Scientific Reports*, 12(1), 1–12. <https://doi.org/10.1038/s41598-022-16612-6>
- Liu, C., Lin, Q., & Yun, Z. (2015). Cellular and Molecular Mechanisms Underlying Oxygen-Dependent Radiosensitivity. *Radiation Research*, 183(5), 487–496, 410. <https://doi.org/10.1667/RR13959.1>

[24]

- Montay-Gruel, P., Bouchet, A., Jaccard, M., Patin, D., Serduc, R., Aim, W., ... & Vozenin, M. C. (2018). X-rays can trigger the FLASH effect: Ultra-high dose-rate synchrotron light source prevents normal brain injury after whole brain irradiation in mice. *Radiotherapy and Oncology*, 129(3), 582-588. <https://doi.org/10.1016/j.radonc.2018.08.016>
- Pratx, G., & Kapp, D. S. (2019). A computational model of radiolytic oxygen depletion during FLASH irradiation and its effect on the oxygen enhancement ratio. *Physics in Medicine & Biology*, 64(18), 185005. <https://doi.org/10.1088/1361-6560/ab3769>
- Sørensen, B. S., Sitarz, M. K., Ankjærgaard, C., Johansen, J., Andersen, C. E., Kanouta, E., ... & Poulsen, P. (2022). *In vivo* validation and tissue sparing factor for acute damage of pencil beam scanning proton FLASH. *Radiotherapy and Oncology*, 167, 109-115. <https://doi.org/10.1016/j.radonc.2021.12.022>
- Tinganelli, W., Weber, U., Puspitasari, A., Simoniello, P., Abdollahi, A., Oppermann, J., ... & Durante, M. (2022). FLASH with carbon ions: Tumor control, normal tissue sparing, and distal metastasis in a mouse osteosarcoma model. *Radiotherapy and Oncology*, 175, 185-190. <https://doi.org/10.1016/j.radonc.2022.05.003>
- Town, C. D. (1967). Effect of High Dose Rates on Survival of Mammalian Cells. *Nature*, 215(5103), 847-848. <https://doi.org/10.1038/215847a0>
- Vozenin, M. C., De Fornel, P., Petersson, K., Favaudon, V., Jaccard, M., Germond, J. F., ... & Bourhis, J. (2019). The Advantage of FLASH Radiotherapy Confirmed in Mini-pig and Cat-cancer Patients. *Clinical cancer research: an official journal of the American Association for Cancer Research*, 25(1), 35-42. <https://doi.org/10.1158/1078-0432.CCR-17-3375>
- Weiss, H., Epp, E. R., Heslin, J. M., Ling, C. C., & Santomasso, A. (1974). Oxygen depletion in cells irradiated at ultra-high dose-rates and at conventional dose-rates. *International journal of radiation biology and related studies in physics, chemistry, and medicine*, 26(1), 17-29. <https://doi.org/10.1080/09553007414550901>
- Whillans, D. W., & Rauth, A. M. (1980). An Experimental and Analytical Study of Oxygen Depletion in Stirred Cell Suspensions. *Radiation Research*, 84(1), 97-114. <https://doi.org/10.2307/3575221>

[25]

## CURRICULUM VITAE

**Name** : Miss Pharewa Karoon

**Date of Birth** : March 14, 1998

**Place of Birth** : Nakhon Ratchasima, Thailand

**Education** :

2016 - 2019 B.Sc. in Physics (Honors), School of Physics, Suranaree University of Technology, Thailand

2020 - 2022 M.Sc. in Physics, School of Physics, Suranaree University of Technology, Thailand

**Scholarship** :

2016 - Development and Promotion of Science and Technology Talents Project (DPST), Thai Thai government scholarship for graduate honor students of Suranaree University of Technology in Bachelor's and Master's degrees

**Experience** :

2021 Internship and training in the field of cancer therapy as part of the GET INvolved program at the GSI Helmholtz Centre for Heavy Ion Research, Germany

**Publications** :

1. P. Karoon, C. Kobdaj, C. Talabnin, and M. Fuss (2023). Experimental Study of Radiolytic Oxygen Depletion from X-Ray Irradiation in Water and Liquid Samples. **The 8<sup>th</sup> RSU International Research Conference on Sciences and Technology 2023**